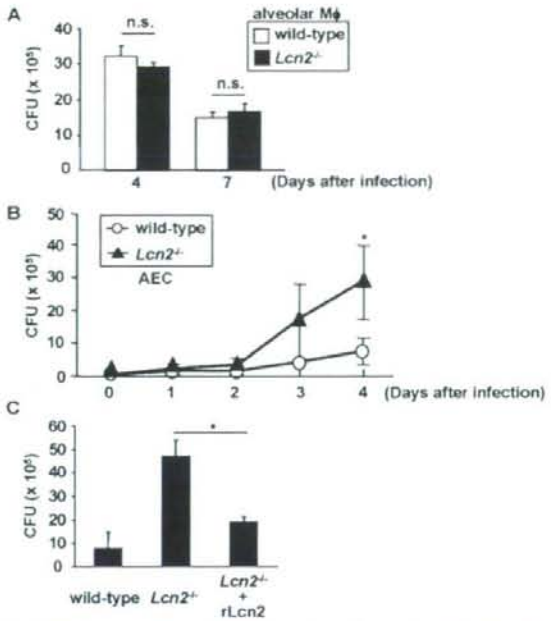

FIGURE 5. Increased BCG growth in $Lcn2^{-/-}$ alveolar epithelial cells. *A*, Alveolar macrophages were collected from uninfected wild-type and $Lcn2^{-/-}$ mice and cultured with BCG for the indicated periods. To eliminate external BCG, the cells were cultured with streptomycin for 1 h, washed three times, and harvested. Lysates of the cells were plated on 7H10-OADC agar, and the CFU numbers were counted. Representative data of two independent experiments are shown. n.s., not significant. *B*, Wild-type and $Lcn2^{-/-}$ AECs were cultured with BCG for the indicated periods. After removal of extracellular BCG, lysates the cells were plated on 7H10-OADC agar, and the CFU numbers were counted. Data are presented as means ± SD of triplicate determinations and are representative of three independent experiments. *, $p < 0.05$. Similar results were obtained when other AECs from wild-type and $Lcn2^{-/-}$ mice were used. *C*, Wild-type and $Lcn2^{-/-}$ AECs were cultured with BCG. At 2 days after infection, rLcn2 (final concentration 30 μg/ml) was added to the $Lcn2^{-/-}$ AEC. After an additional 2 days of culture, the cells were incubated with streptomycin for 1 h, washed three times, and harvested. Lysates of the cells were plated on 7H10-OADC agar, and the CFU numbers were counted. Representative data of three independent experiments are shown. Data are presented as means ± SD of triplicate determinations. *, $p < 0.05$.

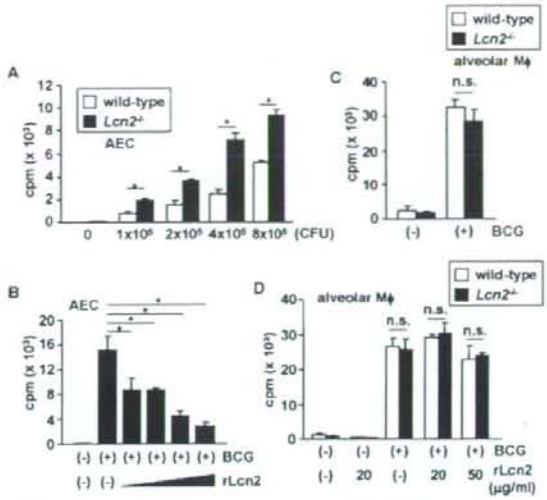

FIGURE 6. Lcn2-mediated inhibition of intracellular BCG growth. *A*, Wild-type and $Lcn2^{-/-}$ AECs were seeded onto 96-well plates and infected with the indicated CFUs of BCG for 6 h. The cells were then extensively washed to remove extracellular BCG and cultured in the presence of [^{3}H]uracil for 48 h. The incorporation of [^{3}H]uracil was measured. Data are presented as means ± SD of triplicate samples. Representative data of three independent experiments are shown. *, $p < 0.005$. *B*, $Lcn2^{-/-}$ AECs were seeded onto 96-well plates, and infected with BCG (2×10^5 CFU) for 6 h. After vigorous washing, the cells were cultured with increasing concentrations of rLcn2 (20, 30, 40, and 50 μg/ml) and [^{3}H]uracil for 48 h, before being measured for their [^{3}H]uracil incorporation. Data are presented as means ± SD of triplicate samples, and are representative of two independent experiments. ∘ indicate a significant difference among groups, ANOVA, posthoc Scheffe, *, $p < 0.001$. *C*, Alveolar macrophages were collected from uninfected wild-type and $Lcn2^{-/-}$ mice, and cultured with BCG for 6 h. After vigorous washing, the cells were cultured in the presence of [^{3}H]uracil for 48 h, before being measured for their [^{3}H]uracil incorporation. Data are presented as the mean ± SD of triplicate samples. n.s., not significant. *D*, Alveolar macrophages from wild-type and $Lcn2^{-/-}$ mice were infected with BCG for 6 h. After vigorous washing, the cells were cultured in the presence of the indicated concentration of rLcn2 and [^{3}H]uracil for 48 h. Then, the [^{3}H]uracil incorporation was counted. Data are presented as means ± SD of triplicate samples. n.s., not significant.

Inhibition of intracellular mycobacterial growth by Lcn2

Mycobacteria are intracellular bacteria that replicate within cells. In the experiments performed so far, it is possible that extracellular growth was monitored as well as intracellular growth under the in vitro conditions. Therefore, to assess the intracellular growth of mycobacteria more precisely, we used [^{3}H]uracil, which is preferentially incorporated into mycobacterial nucleic acids (33). AECs derived from wild-type and $Lcn2^{-/-}$ mice were infected with several CFUs of BCG for 6 h, extensively washed with culture medium containing streptomycin to exclude extracellular BCG, and then cultured for 2 days in the presence of [^{3}H]uracil (Fig. 6*A*). Under these conditions, [^{3}H]uracil incorporation was below 1×10^2 cpm in wells containing uninfected AECs or wells placed in contact with BCG and then extensively washed. After infection with each CFU, [^{3}H]uracil incorporation was increased in $Lcn2^{-/-}$ cells compared with wild-type cells. In BCG-infected $Lcn2^{-/-}$ cells, addition of exogenous rLcn2 reduced the uptake of [^{3}H]uracil by intracellular BCG (Fig. 6*B*). In alveolar macrophages, the [^{3}H]uracil incorporation by intracellular BCG was comparable between wild-type and $Lcn2^{-/-}$ cells (Fig. 6*C*). Addition of rLcn2 did not effectively reduce the uptake of [^{3}H]uracil by intracellular BCG in alveolar macrophages from both wild-type and $Lcn2^{-/-}$ mice (Fig. 6*D*). These findings indicate that extracellular Lcn2 limits intracellular growth of BCG in AECs, but not in alveolar macrophages.

Because extracellular Lcn2 modulated intracellular mycobacterial growth in the AECs, we analyzed whether extracellular Lcn2 was incorporated into the AECs as described in several previous reports (18, 19). AECs were infected with GFP-expressing BCG and then treated with fluorescein-labeled rLcn2 (Fig. 7*A*). Lcn2 was detected within the AECs, and colocalized with dextran that was taken up into the cells by endocytosis. Furthermore, many BCG were colocalized with rLcn2, indicating that endocytosed Lcn2 was in close proximity to intracellular BCG. In contrast, although Lcn2 was incorporated into alveolar macrophages, the incorporated Lcn2 was not colocalized with BCG in alveolar macrophages (Fig. 7*B*), indicating that BCG and rLcn2 were localized in distinct cellular compartments within macrophages. We blocked

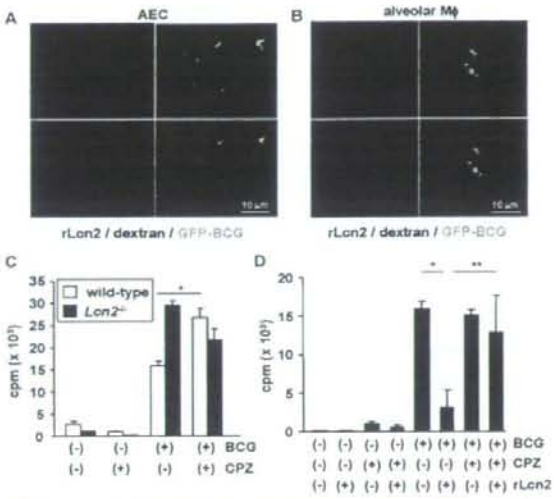

FIGURE 7. Requirement of Lcn2 incorporation for the inhibition of intracellular BCG growth. *A*, GFP-expressing BCG (green)-infected alveolar epithelial cells were cultured with dextran (25 μg/ml; blue) and fluorescein-labeled rLcn2 (15 μg/ml; red) for 6 h. The cells were then washed, fixed with 4% PFA, and analyzed by confocal microscopy. Data are representative of three independent experiments. *B*, GFP-expressing BCG (green)-infected alveolar macrophages were cultured with dextran (25 μg/ml; blue) and fluorescein-labeled rLcn2 (15 μg/ml; red) for 6 h. The cells were then washed, fixed with 4% PFA for 5 min, and analyzed by confocal microscopy. *C*, Wild-type and $Lcn2^{-/-}$ AECs were seeded onto 96-well plates and infected with BCG (2×10^5 CFU) for 6 h. After extensive washing, the cells were cultured with CPZ (10 μM) and [^{3}H]uracil for 48 h. The [^{3}H]uracil incorporation was then measured. Data are presented as means ± SD of triplicate samples, and are representative of two independent experiments. *, $p < 0.01$. *D*, $Lcn2^{-/-}$ AECs were seeded onto 96-well plates, and infected with BCG for 6 h. After washing, the cells were cultured with CPZ for 30 min and then cultured with rLcn2 (20 μg/ml) and [^{3}H]uracil for 48 h. The [^{3}H]uracil incorporation was measured. Data are presented as means ± SD of triplicate samples, and are representative of two independent experiments. * or ** indicate a significant difference among groups, ANOVA, posthoc Scheffe, *, $p < 0.005$; **, $p < 0.05$.

endocytosis of Lcn2 using CPZ after BCG infection. Addition of CPZ resulted in increased BCG growth in wild-type AECs, but not in $Lcn2^{-/-}$ cells (Fig. 7*C*). We also analyzed the effects of the endocytosis inhibitor on rLcn2-mediated inhibition of BCG growth (Fig. 7*D*). Addition of CPZ abolished Lcn2-mediated inhibition of [^{3}H]uracil incorporation in both wild-type and $Lcn2^{-/-}$ cells. Cytochalasin B, which also blocks endocytosis, had similar effects to those of CPZ on Lcn2-mediated inhibition of intracellular BCG growth (data not shown). These findings indicate that endocytosed Lcn2 inhibits the intracellular growth of BCG in AECs.

Discussion

Lcn2 has a variety of putative functions, as evident from its many different names such as neutrophil gelatinase-associated lipocalin, uterocalin, 24p3, and siderocalin (12, 13, 16, 19). In the context of its function in host defense, a structural study of the Lcn2 protein revealed that it associates with enterobactin-type bacterial siderophores (16). Subsequently, Lcn2 was shown to bind to several types of siderophores such as caroboxy-mycobactin and bacillibactin (20, 21). In addition, Lcn2 has been proposed to bind to an as-yet unknown mammalian siderophore (18, 34). Thus, Lcn2 has the ability to bind to a variety of types of siderophores. Furthermore, Lcn2 has been shown to inhibit the growth of *E. coli* through sequestration of iron uptake (22, 23). The present study has demonstrated that Lcn2 also participates in the inhibition of mycobacterial growth through similar mechanisms to those against *E. coli*. Indeed, Lcn2 has been shown to associate with the mycobacteria-derived hydrophilic siderophore carboxy-mycobactin (21). In accordance with our results, Lcn2 has been shown to be secreted from neutrophils during *M. tuberculosis* infection and inhibit their growth (35). Lcn2 was originally identified as a molecule that is secreted from neutrophils, which are rapidly recruited to *M. tuberculosis*-infected lungs. Therefore, neutrophils are presumably the source of Lcn2 as well as alveolar macrophages and epithelial cell during *M. tuberculosis* infection.

Regarding the high sensitivity of $Lcn2^{-/-}$ mice to *M. tuberculosis* infection, it is noteworthy that $Lcn2^{-/-}$ alveolar epithelial cells, but not macrophages, contained increased numbers of *M. tuberculosis* at the early phase of the infection, as evaluated by histopathological and immunohistochemical analyses. This finding was unexpected, because successful in vivo detection of mycobacteria in respiratory epithelial cells in wild-type mice has only been achieved through analyses of mycobacterial DNA or use of electron microscopy, even though mycobacteria have been shown to invade epithelial cells as well as macrophages in vitro (6–9, 36). In addition, $Lcn2^{-/-}$ alveolar epithelial cells, but not macrophages, exhibited defective inhibition of intracellular mycobacterial growth, suggesting that impaired inhibition of mycobacterial growth in alveolar epithelial cells due to the absence of Lcn2 may be a major cause of the high susceptibility $Lcn2^{-/-}$ mice to *M. tuberculosis* infection. Given that mycobacteria were easily detected in the alveolar epithelial cell layers by a typical histological approach in the absence of Lcn2 and the increased mycobacterial growth was observed in $Lcn2^{-/-}$ epithelial cells, but not in macrophages, epithelial cells may play an important role in the host immune responses against respiratory infection with *M. tuberculosis*.

Mycobacteria replicate within cells in vivo, and several lines of evidence indicate that mycobactin-mediated iron uptake is a prerequisite for intracellular mycobacterial growth (27, 29). Consistent with previous studies (18, 19), our findings indicated that Lcn2 is internalized into alveolar epithelial cells via endocytosis. Furthermore, addition of rLcn2 effectively inhibited intracellular mycobacterial growth in AECs, and this effect was abolished by endocytosis inhibitors. At present, it remains unclear how mycobacteria take up iron within epithelial cells using mycobactin. First, it is apparent that mycobacteria exist in the phagosome of macrophages. However, the subcellular localization of mycobacteria within epithelial cells has not been established, although mycobacteria have been shown to be localized in endosomes or macropinosomes (37, 38). Our results revealed colocalization of mycobacteria and dextran, indicating that mycobacteria exist in the endosome-like vacuole within epithelial cells. Second, it remains obscure whether mycobacteria secrete water-soluble carboxy-mycobactin into the cytoplasm to bind the cytosolic iron. It is also obscure how endocytosed Lcn2 approaches the carboxy-mycobactin/iron complexes within the cells. Given that Lcn2 and mycobacteria are colocalized within the endosome-like structure, it is possible that mycobacteria take up the iron entering the endosome using mycobactin, and endocytosed Lcn2, in turn, binds to the carboxy-mycobactin/iron complexes, thereby blocking iron acquisition by mycobacteria. Further studies are required to clarify the precise mechanisms for the interaction between Lcn2 and mycobacteria-derived carboxy-mycobactin.

In alveolar macrophages, the absence of Lcn2 did not affect the sensitivity to mycobacterial infection. This may be due to the differential localizations of mycobacteria in epithelial cells and macrophages. Lcn2 was colocalized with mycobacteria in epithelial

cells, indicating that mycobacteria exist within the endosome-like structure. In contrast, mycobacteria were localized within the phagosome in macrophages, leading to distinct localizations of Lcn2 and mycobacteria in macrophages. Alternatively, macrophages are professional cells that kill intracellular bacteria by producing several macrophage-specific anti-microbial mediators, including NO synthase and Nramp1 (39–41). These mediators may compensate the Lcn2 deficiency in macrophages. In contrast, they are not expressed in epithelial cells, resulting in the high sensitivity to mycobacterial infection in the absence of Lcn2. Thus, in alveolar epithelial cells, Lcn2 may be a major factor that mediates host resistance to mycobacterial infection.

Our results highlight a novel innate host defense system that inhibits mycobacterial infection at the respiratory mucosal surface. We would like to propose the following scenario with regard to the function of Lcn2. Lcn2 is secreted into the alveolar space by alveolar macrophages and epithelial cells during the early phase of respiratory mycobacterial infection. Lcn2 presumably inhibits mycobacterial growth within the alveolar space. In addition, Lcn2 is internalized into the alveolar epithelial cells, which are invaded by mycobacteria, and inhibits mycobacterial growth by sequestering iron uptake. This leads to a reduction in the number of infected mycobacteria at the early phase of infection, which may help to create sufficient time for effective activation of anti-mycobacterial innate and adaptive immune responses. Thus, respiratory epithelial cells play an active role in the resistance to mycobacterial infection, in addition to their functions as physical barriers and secretors of anti-bacterial mediators.

Acknowledgments

We thank I. Sugawara for providing the *M. tuberculosis* H37Rv, Y. Yamada and K. Takeda for technical assistance, and M. Kurata and M. Yasuda for secretarial assistance.

Disclosures

The authors have no financial conflict of interest.

References

1. North, R. J., and Y. J. Jung. 2004. Immunity to tuberculosis. *Annu. Rev. Immunol.* 22: 599–623.
2. Kaufmann, S. H. 2006. Tuberculosis: back on the immunologists' agenda. *Immunity* 24: 351–357.
3. Quesniaux, V., C. Fremond, M. Jacobs, S. Parida, D. Nicolle, V. Yeremeev, F. Bihl, F. Erard, T. Botha, M. Drennan, et al. 2004. Toll-like receptor pathways in the immune responses to mycobacteria. *Microbes Infect.* 6: 946–959.
4. Fremond, C. M., V. Yeremeev, D. M. Nicolle, M. Jacobs, V. F. Quesniaux, and B. Ryffel. 2004. Fatal *Mycobacterium tuberculosis* infection despite adaptive immune response in the absence of MyD88. *J. Clin. Invest.* 114: 1790–1799.
5. Aoki, K., S. Matsumoto, Y. Hirayama, T. Wada, Y. Ozeki, M. Niki, P. Domenech, K. Umemori, S. Yamamoto, A. Mineda, et al. 2004. Extracellular mycobacterial DNA-binding protein 1 participates in mycobacterium-lung epithelial cell interaction through hyaluronic acid. *J. Biol. Chem.* 279: 39798–39806.
6. Teitelbaum, R., W. Schubert, L. Gunther, Y. Kress, F. Macaluso, J. W. Pollard, D. N. McMurray, and B. R. Bloom. 1999. The M cell as a portal of entry to the lung for the bacterial pathogen *Mycobacterium tuberculosis*. *Immunity* 10: 641–651.
7. Bermudez, L. E., and F. J. Sangari. 2001. Cellular and molecular mechanisms of internalization of mycobacteria by host cells. *Microbes Infect.* 3: 37–42.
8. Bermudez, L. E., F. J. Sangari, P. Kolonoski, M. Petrofsky, and J. Goodman. 2002. The efficiency of the translocation of *Mycobacterium tuberculosis* across a bilayer of epithelial and endothelial cells as a model of the alveolar wall is a consequence of transport within mononuclear phagocytes and invasion of alveolar epithelial cells. *Infect. Immun.* 70: 140–146.
9. Hernandez-Pando, R., M. Jeyanathan, G. Mengistu, D. Aguilar, H. Orozco, M. Harboe, G. A. Rook, and G. Bjune. 2000. Persistence of DNA from *Mycobacterium tuberculosis* in superficially normal lung tissue during latent infection. *Lancet* 356: 2133–2138.
10. Ferguson, J. S., and L. S. Schlesinger. 2000. Pulmonary surfactant in innate immunity and the pathogenesis of tuberculosis. *Tuber. Lung Dis.* 80: 173–184.
11. Kjeldsen, L., J. B. Cowland, and N. Borregaard. 2000. Human neutrophil gelatinase-associated lipocalin and homologous proteins in rat and mouse. *Biochim. Biophys. Acta* 1482: 272–283.
12. Devireddy, L. R., J. G. Teodoro, F. A. Richard, and M. R. Green. 2001. Induction of apoptosis by a secreted lipocalin that is transcriptionally regulated by IL-3 deprivation. *Science* 293: 829–834.
13. Kjeldsen, L., A. H. Johnsen, H. Sengelov, and N. Borregaard. 1993. Isolation and primary structure of NGAL, a novel protein associated with human neutrophil gelatinase. *J. Biol. Chem.* 268: 10425–10432.
14. Flower, D. R., A. C. North, and T. K. Attwood. 1991. Mouse oncogene protein 24p3 is a member of the lipocalin protein family. *Biochem. Biophys. Res. Commun.* 180: 69–74.
15. Liu, Q., J. Ryon, and M. Nilsen-Hamilton. 1997. Uterocalin: a mouse acute phase protein expressed in the uterus around birth. *Mol. Reprod. Dev.* 46: 507–514.
16. Goetz, D. H., M. A. Holmes, N. Borregaard, M. E. Bluhm, K. N. Raymond, and R. K. Strong. 2002. The neutrophil lipocalin NGAL is a bacteriostatic agent that interferes with siderophore-mediated iron acquisition. *Mol. Cell* 10: 1033–1043.
17. Nilsen-Hamilton, M., Q. Liu, J. Ryon, L. Bendickson, P. Lepont, and Q. Chang. 2003. Tissue involution and the acute phase response. *Ann. NY Acad. Sci.* 995: 94–108.
18. Devireddy, L. R., C. Gazin, X. Zhu, and M. R. Green. 2005. A cell-surface receptor for lipocalin 24p3 selectively mediates apoptosis and iron uptake. *Cell* 123: 1293–1305.
19. Yang, J., D. Goetz, J. Y. Li, W. Wang, K. Mori, D. Setlik, T. Du, H. Erdjument-Bromage, P. Tempst, R. Strong, and J. Barasch. 2002. An iron delivery pathway mediated by a lipocalin. *Mol. Cell* 10: 1045–1056.
20. Abergel, R. J., M. K. Wilson, J. E. Arceneaux, T. M. Hoette, R. K. Strong, B. R. Byers, and K. N. Raymond. 2006. Anthrax pathogen evades the mammalian immune system through stealth siderophore production. *Proc. Natl. Acad. Sci. USA* 103: 18499–18503.
21. Holmes, M. A., W. Paulsene, X. Jide, C. Ratledge, and R. K. Strong. 2005. Siderocalin (Lcn 2) also binds carboxymycobactins, potentially defending against mycobacterial infections through iron sequestration. *Structure* 13: 29–41.
22. Flo, T. H., K. D. Smith, S. Sato, D. J. Rodriguez, M. A. Holmes, R. K. Strong, S. Akira, and A. Aderem. 2004. Lipocalin 2 mediates an innate immune response to bacterial infection by sequestrating iron. *Nature* 432: 917–921.
23. Berger, T., A. Togawa, G. S. Duncan, A. J. Elia, A. You-Ten, A. Wakeham, H. E. Fong, C. C. Cheung, and T. W. Mak. 2006. Lipocalin 2-deficient mice exhibit increased sensitivity to *Escherichia coli* infection but not to ischemia-reperfusion injury. *Proc. Natl. Acad. Sci. USA* 103: 1834–1839.
24. Smith, K. D. 2007. Iron metabolism at the host pathogen interface: lipocalin 2 and the pathogen-associated iroA gene cluster. *Int. J. Biochem. Cell Biol.* 39: 1776–1780.
25. Houben, E. N., L. Nguyen, and J. Pieters. 2006. Interaction of pathogenic mycobacteria with the host immune system. *Curr. Opin. Microbiol.* 9: 76–85.
26. De Voss, J. J., K. Rutter, B. G. Schroeder, and C. E. Barry, 3rd. 1999. Iron acquisition and metabolism by mycobacteria. *J. Bacteriol.* 181: 4443–4451.
27. De Voss, J. J., K. Rutter, B. G. Schroeder, H. Su, Y. Zhu, and C. E. Barry, 3rd. 2000. The salicylate-derived mycobactin siderophores of *Mycobacterium tuberculosis* are essential for growth in macrophages. *Proc. Natl. Acad. Sci. USA* 97: 1252–1257.
28. Gobin, J., and M. A. Horwitz. 1996. Exochelins of *Mycobacterium tuberculosis* remove iron from human iron-binding proteins and donate iron to mycobactins in the *M. tuberculosis* cell wall. *J. Exp. Med.* 183: 1527–1532.
29. Luo, M., E. A. Fadeev, and J. T. Groves. 2005. Mycobactin-mediated iron acquisition within macrophages. *Nat. Chem. Biol.* 1: 149–153.
30. Jat, P. S., M. D. Noble, P. Ataliotis, Y. Tanaka, N. Yannoutsos, L. Larsen, and D. Kioussis. 1991. Direct derivation of conditionally immortal cell lines from an H-2Kb-tsA58 transgenic mouse. *Proc. Natl. Acad. Sci. USA* 88: 5096–5100.
31. Whitehead, R. H., P. E. VanEeden, M. D. Noble, P. Ataliotis, and P. S. Jat. 1993. Establishment of conditionally immortalized epithelial cell lines from both colon and small intestine of adult H-2Kb-tsA58 transgenic mice. *Proc. Natl. Acad. Sci. USA* 90: 587–591.
32. deMello, D. E., S. Mahmoud, P. J. Padfield, and J. W. Hoffmann. 2000. Generation of an immortal differentiated lung type-II epithelial cell line from the adult H-2K(b)tsA58 transgenic mouse. *In Vitro Cell. Dev. Biol. Anim.* 36: 374–382.
33. Rook, G. A., B. R. Champion, J. Steele, A. M. Varey, and J. L. Stanford. 1985. I-A restricted activation by T cell lines of anti-tuberculosis activity in murine macrophages. *Clin. Exp. Immunol.* 59: 414–420.
34. Mori, K., H. T. Lee, D. Rapoport, I. R. Drexler, K. Foster, J. Yang, K. M. Schmidt-Ott, X. Chen, J. Y. Li, S. Weiss, et al. 2005. Endocytic delivery of lipocalin-siderophore-iron complex rescues the kidney from ischemia-reperfusion injury. *J. Clin. Invest.* 115: 610–621.
35. Martineau, A. R., S. M. Newton, K. A. Wilkinson, B. Kampmann, B. M. Hall, N. Nawroly, G. E. Packe, R. N. Davidson, C. J. Griffiths, and R. J. Wilkinson. 2007. Neutrophil-mediated innate immune resistance to mycobacteria. *J. Clin. Invest.* 117: 1988–1994.
36. Sato, K., H. Tomioka, T. Shimizu, T. Gonda, F. Ota, and C. Sano. 2002. Type II alveolar cells play roles in macrophage-mediated host innate resistance to pulmonary mycobacterial infections by producing proinflammatory cytokines. *J. Infect. Dis.* 185: 1139–1147.
37. Bermudez, L. E., and J. Goodman. 1996. *Mycobacterium tuberculosis* invades and replicates within type II alveolar cells. *Infect. Immun.* 64: 1400–1406.
38. Garcia-Perez, B. E., R. Mondragon-Flores, and J. Luna-Herrera. 2003. Internalization of *Mycobacterium tuberculosis* by macropinocytosis in non-phagocytic cells. *Microb. Pathog.* 35: 49–55.
39. Adams, D. O., and T. A. Hamilton. 1984. The cell biology of macrophage activation. *Annu. Rev. Immunol.* 2: 283–318.
40. MacMicking, J., Q. W. Xie, and C. Nathan. 1997. Nitric oxide and macrophage function. *Annu. Rev. Immunol.* 15: 323–350.
41. Govoni, G., and P. Gros. 1998. Macrophage NRAMP1 and its role in resistance to microbial infections. *Inflamm. Res.* 47: 277–284.

THE JOURNAL OF BIOLOGICAL CHEMISTRY VOL. 283, NO. 43, pp. 28835–28841, October 24, 2008

Mycolyltransferase-mediated Glycolipid Exchange in Mycobacteria*

Received for publication, July 28, 2008, and in revised form, August 14, 2008 Published, JBC Papers in Press, August 14, 2008, DOI 10.1074/jbc.M805776200

Isamu Matsunaga[‡§], Takashi Naka[¶], Rahul S. Talekar[‖], Matthew J. McConnell[‖], Kumiko Katoh[‡§], Hitomi Nakao[‡§], Atsushi Otsuka[‡], Samuel M. Behar[‖], Ikuya Yano[¶], D. Branch Moody[‖], and Masahiko Sugita[‡§1]

From the [‡]Laboratory of Cell Regulation, Institute for Virus Research and [§]Laboratory of Cell Regulation and Molecular Network, Graduate School of Biostudies, Kyoto University, Kyoto 606-8507, Japan, [¶]Japan BCG Laboratory, Tokyo 204-0022, Japan, and [‖]Division of Rheumatology, Immunology, and Allergy, Brigham and Women's Hospital, Harvard Medical School, Boston, Massachusetts 02115

Trehalose dimycolate (TDM), also known as cord factor, is a major surface glycolipid of the cell wall of mycobacteria. Because of its potent biological functions in models of infection, adjuvancy, and immunotherapy, it is important to determine how its biosynthesis is regulated. Here we show that glucose, a host-derived product that is not readily available in the environment, causes *Mycobacterium avium* to down-regulate TDM expression while up-regulating production of another major glycolipid with immunological roles in T cell activation, glucose monomycolate (GMM). *In vitro*, the mechanism of reciprocal regulation of TDM and GMM involves competitive substrate selection by antigen 85A. The switch from TDM to GMM biosynthesis occurs near the physiological concentration of glucose present in mammalian hosts. We further demonstrate that GMM is produced *in vivo* by mycobacteria growing in mouse lung. These results establish an enzymatic pathway for GMM production. More generally, these observations provide a specific enzymatic mechanism for dynamic alterations of cell wall glycolipid remodeling in response to the transition from noncellular to cellular growth environments, including factors that are monitored by the host immune system.

Mycobacterium avium complex (MAC)[2] includes a group of acid-fast bacteria that distribute widely in natural environments, including soil, water, aerosols, and dust (1). Although less virulent than *Mycobacterium tuberculosis*, these environmental mycobacteria occasionally infect humans, especially patients infected with human immunodeficiency virus type 1, where they represent a major cause of morbidity. The incidence of clinically overt MAC infection has increased significantly in recent years, and because of the multidrug resistance evolved by the microbes, MAC infection is difficult to clear with chemotherapeutic agents. Thus, *M. tuberculosis* and MAC are now the two major groups of mycobacteria species that require further efforts for prevention and treatment. Unlike *M. tuberculosis*, which transmits primarily from individuals with active disease, epidemiologic evidence suggests that such transmission pathways are unlikely for MAC. Rather, MAC infection appears to occur when susceptible individuals are exposed to environmental MAC. These observations predict that, upon infection, environmental MAC should undergo significant adaptive changes to allow its survival and replication within the host.

Mycobacteria possess highly lipid-rich cell walls that are critical not simply for their acid-fast properties but also for their survival and replication. The cell wall contains mycolic acids, an α-alkyl-β-hydroxy fatty acid with extremely long carbon chains ($\sim C_{80}$), which are densely aligned in covalent association with the 6-position of arabinose termini of the underlying arabinogalactan sugar layer or exist as free molecules complexed to sugars, either glucose or trehalose. Arabinogalactan-linked mycolates are proposed to extend outward and interact noncovalently with carbon chains of the so-called surface-exposed glycolipids, including trehalose 6-monomycolate (TMM), trehalose 6,6′-dimycolate (TDM), and glucose 6-monomycolate (GMM), thereby forming the hydrophobic cell wall architecture that is essential for protection against chemical attack, such as reactive oxygen intermediates and hydrolytic enzymes derived from the host cells. Among the most abundant surface-exposed glycolipids is TDM that is biosynthesized from its precursor, TMM, by the mycolyltransferase activity of antigen 85 (Ag85) (2). Many biological functions have been assigned to TDM (3) that may impact on survival of mycobacteria within the host and possibly their virulence. Therefore, it is important to determine how biosynthesis of TDM and other mycolic acid-containing glycolipids is regulated by external factors. GMM exists at varied levels in the mycobacterial cell wall (4, 5). In addition to its role in cell wall barrier functions, GMM is a granuloma-forming agent in mice (6) as well as a CD1b presented antigen in humans (7).

* This work was supported, in whole or in part, by National Institutes of Health Grant R01 07155 (NIAID) (to D. B. M.). This work was also supported by grants-in-aid from scientific research on priority areas from the Ministry of Education, Culture, Sports, Science and Technology (to M. S.), grants-in-aid for scientific research B (to M. S.) and C (to I. M.) from the Japan Society for the Promotion of Science, grants from the Ministry of Health, Labour, and Welfare Research on Emerging and Re-emerging Infectious Diseases (to M. S.), and by the Burroughs Wellcome Fund (to D. B. M.). The costs of publication of this article were defrayed in part by the payment of page charges. This article must therefore be hereby marked "*advertisement*" in accordance with 18 U.S.C. Section 1734 solely to indicate this fact.

The nucleotide sequence(s) reported in this paper has been submitted to the DDBJ/GenBank™/EBI Data Bank with accession number(s) AB325677.

[1] To whom correspondence should be addressed: 53 Kawahara-cho, Shogoin, Sakyo-ku, Kyoto 606-8507, Japan. Fax: 81-75-752-3232; E-mail: msugita@virus.kyoto-u.ac.jp.

[2] The abbreviations used are: MAC, *Mycobacterium avium* complex; Ag85, antigen 85; GC-MS, gas chromatography-mass spectrometry; GMM, glucose 6-monomycolate; IL-2, interleukin-2; MALDI-TOF MS, matrix-assisted laser desorption ionization-time of flight mass spectrometry; TCR, T cell receptor; TDM, trehalose 6,6′-dimycolate; TMM, trehalose 6-monomycolate; LC-MS, liquid chromatography-mass spectrometry.

Here we identify Ag85A as an enzyme that produces GMM by transfer of mycolate to glucose. Furthermore, mechanistic studies show that glucose present in its growth environment regulates the spectrum of mycolylglycolipids made by MAC, and glucose from the host influences GMM production *in vivo* during infection of mice. Mechanistic studies showed that glucose and trehalose compete as substrates for Ag85A, linking the biosynthesis pathways of GMM and TDM.

EXPERIMENTAL PROCEDURES

Reagents and Bacteria—Chemical reagents were purchased from Nacalai Tesque (Kyoto, Japan) unless otherwise indicated. *M. avium* ATCC 35767 (serovar 4) was obtained from American Type Culture Collection (Manassas, VA). The bacteria were maintained on a plate of Middlebrook 7H10 media supplemented with 10% oleic acid/albumin/dextrose/catalase (BD Biosciences). For extraction of the total lipid fraction, the bacteria were cultured in Middlebrook 7H9 broth media (containing 0.05% Tween 80 but not glycerol) supplemented with 10% albumin/dextrose/catalase (BD Biosciences). The log phase culture was diluted with 20 volumes of 7H9 media containing various concentrations of glucose, and the culture was continued for another 5–7 days until the absorbance at 600 nm reached ~1. In some experiments, bacteria were grown in media containing either 0.01 or 0.1% glucose, and the media were replaced every day with fresh media containing the same concentrations of glucose. After 5 days, the bacteria were harvested for lipid extraction. To monitor early GMM production, bacteria were grown either in 7H9 media containing 0.01 or 0.1% glucose or in human serum and were harvested after 2, 4, 8, 18, and 24 h of culture.

Preparation of Mycolylglycolipids from MAC—Total lipids from mycobacteria were prepared as described previously (8). The total lipids were then dissolved in chloroform/methanol (C/M, 2:1, v/v), and 20 volumes of ice-cold acetone were added. After 30 min of incubation on ice, the suspension was subjected to centrifugation at 1,500 × *g* for 15 min at 1 °C, and the supernatant was carefully removed. The pellet was then washed with ice-cold acetone, and the residue was dissolved in C/M (2:1) and fractionated by TLC using an Analtech TLC plate (Newark, DE) with a solvent system of chloroform/methanol/acetone/acetic acid (90:10:10:1, v/v). GMM, TDM and TMM fractions were extracted with C/M (2:1) from the silica gels. For GMM and TDM purification, the fractions were further fractionated by TLC with a solvent system of chloroform/acetone/methanol/water (50:60:2.5:0.6, v/v). Finally, the GMM, TDM and TMM fractions were extracted with C/M (2:1), dried, and rinsed several times with methanol at room temperature to remove any residual contamination of glycopeptidolipids and phospholipids.

Matrix-assisted Laser Desorption Ionization-Time of Flight Mass Spectrometry (MALDI-TOF MS)—MALDI-TOF MS analyses of glycolipids were carried out according to the method described previously (9). Briefly, MALDI-TOF MS spectra were acquired on a Voyager DE-STR MALDI-TOF mass spectrometer (Applied Biosystems) with a pulse laser emitting at 337 nm. Samples were analyzed in the reflectron mode with an accelerating voltage operating in positive ion mode of 20 kV. As the matrix, 2,5-dihydroxybenzoic acid was used.

Gas Chromatography-Mass Spectrometry (GC-MS)—GC-MS analysis of the sugar moiety of GMM was carried out according to the method described previously (9). Briefly, GMM was hydrolyzed with 2 M trifluoroacetic acid at 120 °C for 2 h. The aqueous phase was dried, reduced with 10 mg/ml solution of $NaBD_4$ (1 M NH_4OH/C_2H_5OH, 1:1, v/v) at room temperature for 2 h, and then acetylated with acetic anhydride/pyridine (1:1, v/v) at 100 °C for 1 h. The resulting alditol acetate derivatives were analyzed by GC-MS with GCMS-QP2010 plus (Shimazu Co., Ltd., Kyoto, Japan), using a fused silica capillary column (SP-2380, 30 m × 0.25 mm inner diameter; Supelco Inc.). GC oven was operated at 50 °C for 0.5 min, and then the temperature was increased to 235 °C at a rate of 65 °C/s. The temperature was then kept at 235 °C for 12 min. Flow rate of helium gas was 44.4 cm/min.

Isolation of the Antigen 85A Gene from MAC, Preparation of the Recombinant Enzyme and Its Enzymatic Assay—The genomic DNA was isolated from the MAC strain using the Isoplant kit according to the manufacturer's instruction (Wako Pure Chemical Co. Ltd., Osaka, Japan). The gene that encoded the mature Ag85A lacking the signal sequence was amplified by PCR, using a specific primer set as follows: 5′-gga att cca tat gtt ctc gcg ccc cgg tct gcc-3′ (a sense primer, in which the NdeI restriction site is underlined) and 5′-ccg ctc gag ggt gcc ctgg ccg ttc ccg g-3′ (an antisense primer, in which the XhoI restriction site is underlined). PCR was carried out using a Takara LA-*Taq*DNA polymerase (Takara Co. Ltd., Tokyo, Japan), and the cycling conditions for PCR amplification were as follows: 94 °C, 2 min, followed by 30 cycles of 98 °C, 20 s and 72 °C, 1.5 min, and a final extension step of 72 °C, 3 min. The amplified PCR products were digested with NdeI and XhoI and ligated to a NdeI-XhoI-digested pET-21c plasmid vector (Merck). The nucleotide sequences of the Ag85A gene were determined for four isolated clones. *Escherichia coli* BL21 (DE3) was transformed with the Ag85A gene in pET-21c, and induction of protein expression was performed according to a method of Kremer *et al.* (10).

The bacteria expressing the His-tagged mature Ag85A were harvested and disrupted by sonication in ice-cold 20 mM Tris-HCl buffer (pH 7.9) containing 0.5 M NaCl and 60 mM imidazole (sonication buffer). The sonicate was centrifuged at 10,000 × *g* for 30 min at 4 °C to remove insoluble materials, and then the supernatant was applied onto a Ni^{2+}-resin column equilibrated with the sonication buffer at 4 °C. After washing the column with the sonication buffer, the recombinant Ag85A was eluted with 20 mM Tris-HCl buffer (pH 7.9) containing 0.5 M NaCl and 0.5 M imidazole. The eluate was concentrated and dialyzed against 50 mM Tris-HCl buffer (pH 7.4) containing 10% glycerol overnight at 4 °C. Protein concentration of the recombinant Ag85A preparation was determined by the Quick Start Bradford protein assay kit (Bio-Rad). Purity of the preparation was determined by SDS-PAGE and Coomassie staining.

Mycolyltransferase assays were carried out by modification of a method of Kremer *et al.* (10). Twenty μg of purified TMM was dispersed by sonication in 150 μl of 50 mM sodium phosphate buffer (pH 7.4) in the presence or absence of indicated

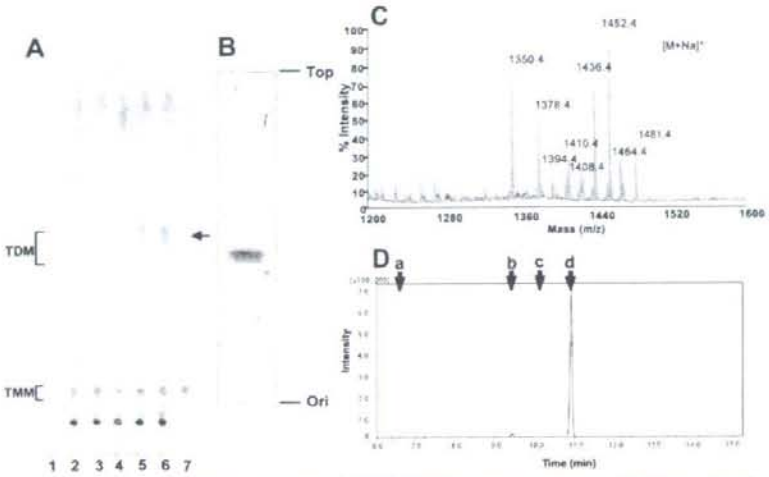

FIGURE 1. **A reciprocal production of TDM and GMM in MAC in response to glucose.** *A*, MAC was cultured in media containing 0.01% (w/v, *lane 2*), 1% (w/v, *lane 3*), 2% (w/v, *lane 4*), 5% (w/v, *lane 5*), and 10% glucose (w/v, *lane 6*), and the total lipid fractions (50 μg each) were analyzed on a TLC plate that was developed with chloroform/methanol/acetone/acetic acid (90:10:10:1, v/v). Purified TDM (*lane 1*) and TMM (*lane 7*) were used as references. Glucose dose-dependent production of a lipid species (indicated with an *arrow*) was detected. *B*, lipid species was purified and analyzed on a silica gel TLC plate that was developed with chloroform/methanol (9:1, v/v). *C*, MALDI-TOF MS profiles of the purified lipid species. *D*, GC-MS analysis of the sugar moiety of the purified lipid species. *Arrows* indicate retention times for the alditol acetate derivatives of arabinose (*a*), mannose (*b*), galactose (*c*)/ and glucose (*d*). Ion chromatogram of *m/z* 290 is shown. The retention time of the major ion corresponded with that of a glucose alditol acetate derivative.

concentration of D-glucose. The reaction was started by the addition of 50 μl of the enzyme preparation containing 50 μg of protein. After 1 h of incubation at 37 °C, the reaction was stopped by the addition of 2 ml of C/M (2:1) and 0.3 ml of distilled water. The lipids were extracted by the method of Kremer *et al.* (10) and analyzed by silica gel TLC. The lipids on the TLC plate were visualized by spraying 50% sulfuric acid and baking.

GMM Detection in Vivo—Mouse infections were carried out via the aerosol route with 10^2 *M. tuberculosis* Erdman strain with mice sacrificed after ~21 days of infection. Lungs were homogenized with beads and centrifuged at 2000 × *g* for 30 min at room temperature. The bacterial pellet was treated with 2% NaOH to disperse phospholipid bilayers, neutralized with 0.27 M phosphoric acid in phosphate buffered saline, and centrifuged at 2000 × *g* for 30 min to recover bacteria. Lipids were extracted from this mixture with three serial extractions in C/M (2:1, 1:1, and 1:2), evaporated to dryness under nitrogen, and resuspended in 1:1 C/M. These lipids were further fractionated by cold acetone precipitation to enrich for lipids that were analyzed by normal phase chromatography on a diol column. Solvent A was methanol, and solvent B was 60:40 (v/v) hexane/2-propanol. Both solvents contained 0.1% (v/v) formic acid and 0.05% (v/v) ammonium hydroxide. A binary gradient was used beginning at 5% solvent A for 3 min, linearly increasing to 40% solvent A over 5 min, holding at 40% solvent A for 6 min, linearly increasing to 100% solvent A over 2.2 min, holding at 100% solvent A for 3 min, linearly decreasing to 5% solvent A over 3.6 min, and finally holding at 5% solvent A for 3.2 min. Compounds matching the expected mass for GMM were detected at after 3.6–3.9 min of elution under these conditions. The accurate mass experiment was carried out with an Agilent 6520 Accurate Mass QTOF-LC-MS operated in the positive mode with an Agilent Technologies 1200 Series high pressure liquid chromatography system. CID-MS was carried out with a ThermoLCQ Advantage Ion Trap mass spectrometer with nano-electrospray ionization in comparison with GMM derived from *Mycobacterium fallax* (11).

GMM-specific T Cell Assays—The T cell receptor (TCR)-deficient Jurkat cells (J.RT3) reconstituted by transfection with GMM-specific, CD1b-restricted TCRs have been described previously (12). The T cells (5×10^4/well) were cocultured in 96-well microtiter plates with the C1R human B-lymphoblastoid cells (1×10^5/well) stably transfected either with CD1b (C1R/CD1b) or with empty vector alone (C1R/mock) (13) in the presence of phorbol 12-myristate 13-acetate (10 ng/ml) and indicated concentrations of lipid preparations. In some experiments, monocyte-derived dendritic cells were used as antigen-presenting cells. After 20 h, aliquots of the culture supernatants were collected, and the amount of interleukin-2 (IL-2) released into the supernatants was measured by the IL-2 ELISA kit (BD Biosciences).

RESULTS

Reciprocal Production of TDM and GMM by MAC in Response to Glucose—Glucose is an essential nutrient to living organisms, which is utilized as a source not only for energy production but also for biosynthesis of glycosylated constituents of cellular architecture. Unlike other hexose sugars, glucose is maintained at high levels in the blood and tissues of mammalian hosts. Therefore, we predicted that, upon infection into the host, MAC grown in glucose-limited environments might undergo significant alterations in glycolipid biosynthesis by exposure to host-derived glucose. To gain insights into the impact of exogenous glucose on glycolipid composition in mycobacteria, we first monitored glycolipid production by *M. avium* strain (serovar 4) that was harvested after cultivation in liquid media supplemented with different concentrations of glucose. The total lipid fraction was obtained by extracting each bacterial preparation with chloroform and methanol. The lipids were then analyzed on a TLC plate developed with a solvent system suitable for separation of chemically diverse glycolipid species (Fig. 1*A*). When grown in the presence of a trace amount of glucose (0.01%, w/v), mycobacteria produced high levels of TDM and TMM (Fig. 1*A*, *lane 2*, shown with *brackets*). As the glucose concentrations present in media were increased,

TDM production decreased, whereas the amount of TMM remained constant (Fig. 1*A*, *lanes 2–6*). Also, an increase in a discrete, unknown lipid species with a retardation factor (R_f) slightly greater than that of TDM was noted (Fig. 1*A*, *lanes 3–6*, indicated with an *arrow*). To determine the molecular identity of the unknown lipid, it was purified and subjected to TLC and MS analyses. The purified lipid was resolved as doublet bands on a TLC plate developed with a solvent system of C/M (9:1, v/v) (Fig. 1*B*). MALDI-TOF MS analysis revealed that the mass numbers of given ions were matched with those of sodium adducts of hexose monomycolate (Fig. 1*C*). Within the limits of error of the method of detection, the masses matched both in terms of the expected *m/z* of the dominant ions, the range of mass variation expected of individual molecular species of mycolate derivatives, and the absolute mass differences among the major ions, which can be accounted for by differences in carbon chain length and substitution of R groups (14). For example, *m/z* 1452.4 corresponds to the expected mass of sodium adduct of hexose monomycolate with C_{85} fatty acid and a wax ester-type R group on the meromycolate chain (Fig. 1*C*). GC-MS analysis of an alditol acetate derivative of the sugar moiety derived from the purified lipid identified glucose as the hexose group attached to mycolates (Fig. 1*D*). The doublet bands observed on a TLC plate were thus likely to represent two stereoisomers of mycolates as described previously (5, 15). Finally, the production of GMM in response to added glucose is expected based on the ability of mycobacteria to couple abundant hexose sugars at mycolyl esters (5). These results detected a reciprocal production of TDM and GMM by MAC in response to exogenous glucose without apparent alterations in the steady state levels of TMM. This experiment, carried out in live bacteria, raised the possibility that mycolyltransferases might compete for carbohydrate substrates.

Ag85 Utilized Glucose for GMM Biosynthesis—Mycobacteria-derived mycolyltransferases, known also as Ag85, catalyze the final step of TDM biosynthesis, using TMM as a substrate. Current models of the Ag85-catalyzed reaction predicted that two molecules of TMM are captured in the two substrate-binding pockets of the enzyme, and the mycolyl acyl group of the TMM substrate bound in one substrate-binding pocket (donor site) is transferred to the other TMM substrate bound in the other pocket (acceptor site), resulting in generation of one molecule of TDM and one molecule of trehalose (Fig. 2*A*) (2, 16). Although GMM can be an abundant structure in the cell wall and functions to activate T cells and form granulomas, its mechanism of synthesis was unknown. We hypothesized that GMM biosynthesis could be catalyzed by Ag85 if glucose, instead of TMM, occupied the acceptor site (Fig. 2*B*). To address this possibility, we made recombinant Ag85A enzyme from the *M. avium* strain (serovar 4), and we performed *in vitro* enzymatic reaction experiments. To accomplish this, we first carried out PCR from the genome of the MAC strain as a template, and isolated the Ag85A gene that encoded the mature protein lacking the signal sequence. DNA sequencing of the isolated gene revealed that three nucleotides were altered as compared with the previously reported Ag85A gene derived from *M. avium* serovar 1 strain (17), but the deduced amino acid sequences were identical in both strains. We then constructed an expression plasmid in which the initiation codon was placed at the 5′-end and the sequence encoding a His tag was attached in frame at the 3′-end of the isolated Ag85A gene. The His-tagged enzyme was expressed in *E. coli* and affinity-purified by Ni^{2+}-charged resin column chromatography. The purified material was resolved as a single band with an apparent molecular mass of ~33 kDa on a Coomassie-stained SDS-polyacrylamide gel, consistent with its being the Ag85A protein (Fig. 3*A*). Incubation of TMM *in vitro* in the presence of this

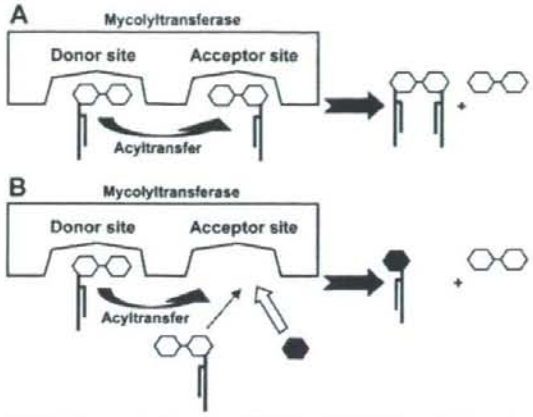

FIGURE 2. **Proposed scheme for TDM (*A*) and GMM (*B*) production catalyzed by mycolyltransferase.** In *model A*, both the donor site and the acceptor site of the enzyme interact with TMM, resulting in TDM formation. In *model B*, a glucose substrate competes against a TMM substrate for access to the acceptor site. When glucose is readily available, glucose rather than TMM preferentially gain access to the site, resulting in production of GMM.

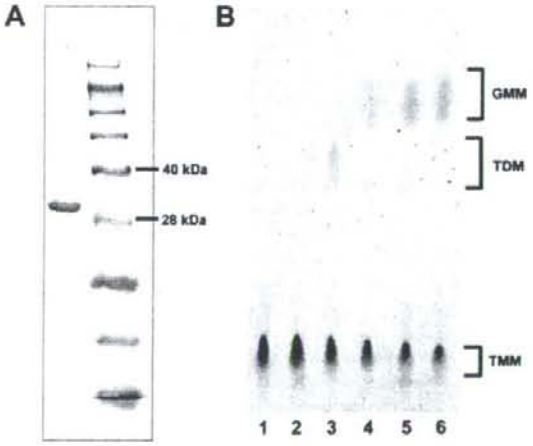

FIGURE 3. **TDM-GMM exchange mediated by recombinant Ag85A.** *A*, purified MAC Ag85A (*left lane*) and a size marker (*right lane*) were resolved on a Coomassie-stained SDS-polyacrylamide gel. Positions for the 40- and 28-kDa marker proteins are indicated. *B*, enzymatic reactions were performed at 37 °C at conditions indicated below, and the lipids were extracted from the reaction mixtures, followed by analysis on a TLC plate. *Lane 1*, Ag85A and TMM with 5% glucose (w/v), 0 h of incubation; *lane 2*, heat-inactivated (100 °C, 3 min) Ag85A and TMM with 5% glucose (w/v), 1 h of incubation; *lanes 3–6*, Ag85A and TMM either with 0.2% (w/v) glucose (*lane 4*), 1% glucose (w/v) (*lane 5*), and 5% (w/v) glucose (*lane 6*) or without glucose (*lane 3*), 1 h of incubation.

enzyme preparation resulted in generation of TDM (Fig. 3*B*, *lane 3*), confirming the mycolyltransferase activity exerted by the recombinant protein. Strikingly, addition of glucose to this reaction condition resulted in decreased TDM production in a dose-dependent manner, which was associated with an increase in GMM (Fig. 3*B*, *lanes 3–6*). GMM synthesis was completely abrogated when heat-inactivated enzyme was used (Fig. 3*B*, *lane 2*). This further confirmed that GMM was produced enzymatically by the mycolyltransferase activity of Ag85A but not as a result of nonenzymatic hydrolysis. These results indicate that Ag85A mediates synthesis of GMM. In this molecular model, we propose that TMM and glucose compete for access to the acceptor site of the Ag85A, and the enzyme preferentially catalyzes biosynthesis of GMM, rather than TDM, when glucose is readily available (Fig. 2*B*). The substrate selection by the mycolyltransferase would likely provide a molecular basis for the glucose-dependent TDM-GMM exchange detected in cultured MAC.

GMM Production Occurs at a Physiological Glucose Concentration—The observations made above have established an enzymatic pathway for GMM production in live mycobacteria that are grown in the presence of high levels of exogenous glucose. However, it remains to be addressed whether mycobacteria can produce GMM under physiological concentrations of glucose present in mammalian hosts, which is maintained at ~100 mg/dl (0.1% w/v). To address this issue, we measured GMM production by mycobacteria cultured in liquid media with a glucose concentration comparable with that in the host. The MAC culture was started in the presence of either 0.01 or 0.1% glucose, and every 24 h, the culture media were replaced with fresh media to maintain the glucose concentrations at constant levels. After 5 days of culture, the bacteria were harvested, and the total lipids were extracted. Subsequently, methanol-insoluble lipids were isolated from these total lipids, followed by separation on TLC plates (Fig. 4*A*). Although TDM production was readily detected in both cultures, GMM production was detected only in the presence of 0.1% glucose (Fig. 4*A*, *lane 2*) but not in the presence of 0.01% glucose (*lane 1*). This was also confirmed by T cell-based assays (Fig. 4*B*) in which Jurkat T cells expressing specific TCRs recognizing GMM in the context of CD1b molecules were used. Incubation of the T cells with CD1b-expressing cells (C1R/CD1b) in the presence of the total lipids from the 0.1% glucose-containing culture resulted in dose-dependent IL-2 production by the T cells, demonstrating high levels of antigenicity when growing at physiological glucose concentrations (Fig. 4*B*, *upper panel*). The specific response was not observed when CD1b-negative cells (C1R/mock) were used as antigen-presenting cells, supporting that the response was CD1b-restricted.

We then addressed how quickly induction of GMM production occurred after exposure to 0.1% glucose. MAC was cultured either in liquid media containing 0.01% (Fig. 5*A*) or 0.1% (*B*) or in human serum (*C*), and the bacteria were harvested at 2, 4, 8, 18, and 24 h. GMM production was observed as early as 8 h after the start of the culture both in 0.1% glucose-containing media and in human serum but not in media containing 0.01% glucose. These observations suggest that GMM production can occur quickly after exposure to high levels of glucose presumably as a result of competitive substrate selection by preexisting mycolyltransferases.

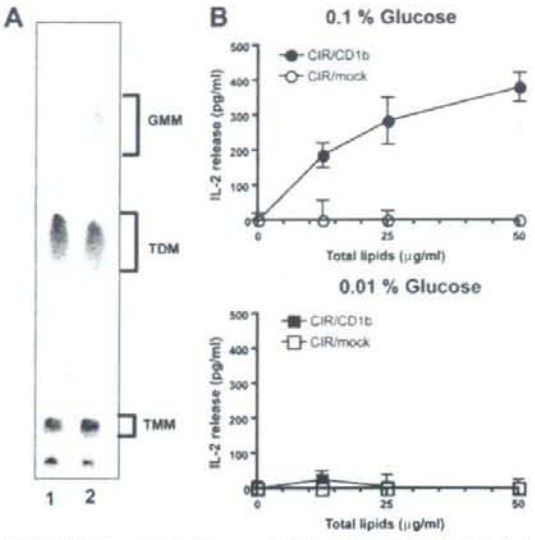

FIGURE 4. **GMM production by mycobacteria cultured at a physiological glucose concentration.** *A*, MAC was cultured in liquid media containing either 0.01 or 0.1% glucose, and the culture media were replaced with fresh media every day to maintain the glucose concentrations. After 5 days, the bacteria were harvested, and the total lipids were extracted. The methanol-insoluble fraction was then obtained from 100 μg of each total lipid preparation and analyzed by TLC. *B*, GMM-specific, CD1b-restricted TCR-expressing Jurkat T cells were cocultured with either C1R/CD1b or C1R/mock in the presence of different concentrations of the total lipids derived from the 0.1% glucose-containing (*upper panel*) and the 0.01% glucose-containing (*lower panel*) cultures. The T cell response was assessed by measuring IL-2 released into the media.

GMM Production Occurs in Mycobacteria-infected Tissues—A previous study detected GMM comigrating lipids can be derived from *Mycobacterium leprae*, raising the possibility that GMM is produced by mycobacteria in tissues (5). However, the chemical structures of such candidate glycosyl mycolates could not be directly determined, and it remained unknown whether *M. tuberculosis* produces GMM during infection. Therefore, we infected CH3 mice with *M. tuberculosis* Erdman strain and isolated mycobacteria directly from the lungs after ~3 weeks of infection. Bacteria were enriched from lung preparations by centrifugation and treatment with weak base to disperse lung tissue. The resulting preparations contained predominantly mycobacterial lipids when analyzed by LC-MS (data not shown). By comparing total *M. tuberculosis* lipids from lung with an *M. fallax* GMM standard in LC-MS experiments, we analyzed the *in vivo* derived lipids that nearly copurified with the GMM standard. Mass measurements with an Accurate Mass QTOF capable of mass resolution of 10 ppm detected an ion at 1317.2577 in lung-derived lipids (Fig. 6*A*). Both the absolute m/z and the isotope ratios matched the predicted masses of an ammonium adduct of a GMM carrying a C_{78} α-mycolic acid within expected error (C_{84}, $H_{162}O_8$, C_{78} GMM, expected m/z 1317.2613). Further supporting the identification of this ion as GMM, mycolic acid derivatives are characteristically synthe-

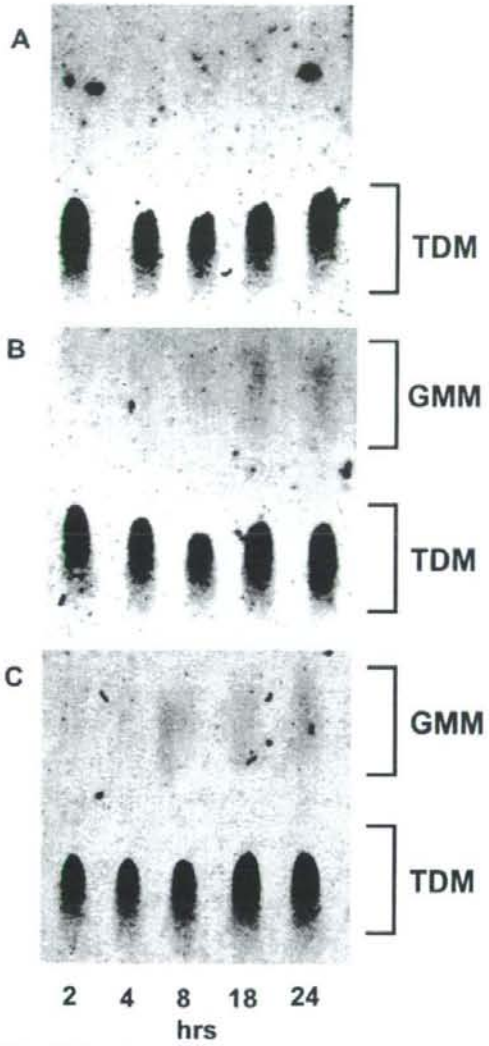

FIGURE 5. **GMM production by mycobacteria during early phases of culture.** MAC was cultured either in liquid media containing 0.01% (*A*) or 0.1% (*B*) glucose or in human serum (*C*). At indicated time points, the bacteria were harvested, and the total lipids were analyzed by TLC.

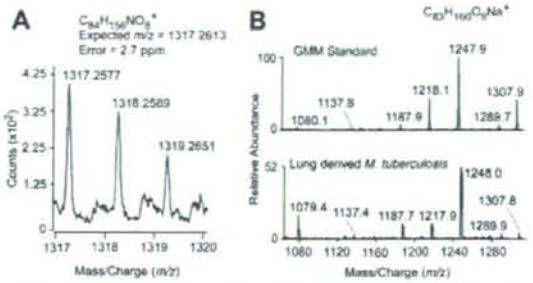

FIGURE 6. **GMM production *in vivo* by *M. tuberculosis*.** *A*, among the mixture of lipids extracted from *M. tuberculosis* derived from mouse lungs, lipids that copurified with a GMM standard were analyzed in the positive mode on an Accurate Mass QTOF MS. The detected mass of *m/z* 1317.2577 corresponds to the predicted mass of an ammonium adduct of C_{78} GMM (*m/z* 1317.2613). *B*, positive mode CID-MS analysis in ion trapping mass spectrometry of *M. fallax* GMM and the lung-derived candidate GMM molecule detected as sodium adducts show a similar pattern of product ions.

sized as a series of molecules that differ from one another by mass increments corresponding to C_2H_2, and the spectrum of the lung-derived lipids contained two additional ions (*m/z* 1345.3033, 1289.2304) corresponding to the expected masses of C_{80} and C_{76} GMM (data not shown). Finally, a separate CID-MS experiment, carried out with an *M. fallax* GMM standard and the lung-derived lipids, showed nearly identical product ions, including ions with mass intervals corresponding to the loss of 60, 90, and 120 units (*m/z* 1248.0, 1217.9, and 1187.7), which likely represent the loss of $C_2H_4O_2$, $C_3H_6O_3$, and $C_4H_8O_4$, which are products expected from cleavage through the hexose sugar (Fig. 6*B*). These data provide strong evidence that GMM is made in the host *in vivo* during an experimental infection.

DISCUSSION

MAC represents a group of environmental mycobacteria that have evolved the capacity to adapt to low nutrition environments. In fact, MAC can survive and replicate in water supply systems (1), where aggregates of the microbes exist in close association with the surface area. This biofilm formation confers significant resistance to a variety of physical and chemical stresses, such as exposure to disinfectants and antibiotics, and thus is an important strategy for the environmental mycobacteria to maintain their life cycles safely in natural environments. These environmental mycobacteria stably express TDM on the surface of their cell wall but fail to biosynthesize GMM because of highly limited availability of glucose. This study argues that, upon entry into the host, this glycolipid phenotype would be modified enzymatically by utilizing the host-derived glucose as a substrate. All three functional mycolyltransferases (Ag85A, Ag85B, and Ag85C) identified in *M. tuberculosis* (18) appear capable of catalyzing TDM synthesis from TMM *in vitro*, and the corresponding Ag85 isoforms have been found also in *M. avium*. Although these enzymes have certain overlapping functions, their differential transcription patterns have been noted in mycobacteria grown under distinct conditions. Ag85A is an isoform that is preferentially expressed in macrophage-resident mycobacteria (19, 20), and thus, its catalytic potential for the TDM-GMM exchange could have an impact on macrophage functions if TDM and GMM have differential ability to activate the cells. Indeed, we recently found that interferon-γ-primed macrophages produced only a marginal level of nitric oxides when stimulated with GMM, which contrasted sharply with those stimulated with TDM that were capable of mounting robust nitric oxide responses (data not shown). Therefore, the TDM-GMM exchange may be valuable in minimizing the nitric oxide response by the host macrophages. Prior to this report, the identity of any mycolyltrans-

ferase that could produce GMM was unknown, so these results establish that Ag85A has this function.

Once pathogens break the frontline defense mediated by the host innate immunity, they are then challenged by specific T lymphocytes that belong to the acquired immunity. Glycolipid-specific T lymphocyte reactions are elicited in humans and guinea pigs infected with mycobacteria, and activation of these T cells is restricted not by the classical major histocompatibility complex-encoded class I and class II molecules but rather by nonmajor histocompatibility complex-encoded group 1 CD1 molecules (CD1a, CD1b, and CD1c in humans) (21). These CD1 molecules are expressed in activated macrophages as well as dendritic cells, the two major cell types for mycobacterial infection. Notably, infiltration of GMM-specific, CD1b-restricted T cells is detected in human skin infected with *M. leprae*, and the human T cell lines (7) and polyclonal T cells (22) exhibit cytotoxic effects, suggesting that the CD1-restricted T cell response directed against GMM could potentially function to clear infection. Taken together, these results raise an interesting possibility that GMM generated as a result of TDM-GMM exchange functions to reduce the innate immune response, but provides the host with a new opportunity to monitor live mycobacteria and eliminate them in the subsequent phases of the acquired immunity. This may represent an example of how the immune system has been constructed during the long processes of evolution to fight efficiently against pathogens.

Despite the fact that GMM is produced by pathogenic mycobacteria and structurally related to the well studied TDM, it has not been the target for focused investigation until recently. Presumably, this is partly because only a tiny amount of GMM, as compared with TDM, is synthesized by pathogenic slow growing mycobacteria, such as *M. tuberculosis* and *M. avium*, when cultured in the Middlebrook "standard" media formulations. Ironically, the standard media used for cultivation of fast growing saprophytic bacteria, such as *Rhodococcus ruber*, contain 1% glucose, and thus, the nonpathogenic bacteria cultured in such a medium produce GMM abundantly, and its structure and biological activities have been studied extensively (6, 23). In many previous studies, the composition, structure, and function of mycobacterial lipids were determined by using bacteria grown in standard media, but the present study suggests that the "lipid world" that is constructed by the bacteria grown in standard culture conditions is substantially different from the lipid world constructed as a result of interaction with the continuously changing host environments.

Acknowledgments—We thank Dr. Seiko Mizuno (Soai University, Osaka, Japan) for use of the GC-MS facility and Dr. Tan-Yun Cheng (Brigham and Women's Hospital, Harvard Medical School, Boston, MA) for reagents and advice.

REFERENCES

1. Primm, T. P., Lucero, C. A., and Falkinham, J. O., III (2004) *Clin. Microbiol. Rev.* **17,** 98–106
2. Sathyamoorthy, N., and Takayama, K. (1987) *J. Biol. Chem.* **262,** 13417–13423
3. Ryll, R., Kumazawa, Y., and Yano, I. (2001) *Microbiol. Immunol.* **45,** 801–811
4. Brennan, P., and Ballou, C. E. (1967) *J. Biol. Chem.* **242,** 3046–3056
5. Moody, D. B., Guy, M. R., Grant, E., Cheng, T. Y., Brenner, M. B., Besra, G. S., and Porcelli, S. A. (2000) *J. Exp. Med.* **192,** 965–976
6. Matsunaga, I., Oka, S., Inoue, T., and Yano, I. (1990) *FEMS Microbiol. Lett.* **55,** 49–53
7. Moody, D. B., Reinhold, B. B., Guy, M. R., Beckman, E. M., Frederique, D. E., Furlong, S. T., Ye, S., Reinhold, V. N., Sieling, P. A., Modlin, R. L., Besra, G. S., and Porcelli, S. A. (1997) *Science* **278,** 283–286
8. Matsunaga, I., Bhatt, A., Young, D. C., Cheng, T. Y., Eyles, S. J., Besra, G. S., Briken, V., Porcelli, S. A., Costello, C. E., Jacobs, W. R., Jr., and Moody, D. B. (2004) *J. Exp. Med.* **200,** 1559–1569
9. Enomoto, Y., Sugita, M., Matsunaga, I., Naka, T., Sato, A., Kawashima, T., Shimizu, K., Takahashi, H., Norose, Y., and Yano, I. (2005) *Biochem. Biophys. Res. Commun.* **337,** 452–456
10. Kremer, L., Maughan, W. N., Wilson, R. A., Dover, L. G., and Besra, G. S. (2002) *Lett. Appl. Microbiol.* **34,** 233–237
11. Cheng, T. Y., Relloso, M., Van Rhijn, I., Young, D. C., Besra, G. S., Briken, V., Zajonc, D. M., Wilson, I. A., Porcelli, S., and Moody, D. B. (2006) *EMBO J.* **25,** 2989–2999
12. Grant, E. P., Degano, M., Rosat, J. P., Stenger, S., Modlin, R. L., Wilson, I. A., Porcelli, S. A., and Brenner, M. B. (1999) *J. Exp. Med.* **189,** 195–205
13. Sugita, M., Porcelli, S. A., and Brenner, M. B. (1997) *J. Immunol.* **159,** 2358–2365
14. Barry, C. E., III, Lee, R. E., Mdluli, K., Sampson, A. E., Schroeder, B. G., Slayden, R. A., and Yuan, Y. (1998) *Prog. Lipid. Res.* **37,** 143–179
15. Natsuhara, Y., Oka, S., Kaneda, K., Kato, Y., and Yano, I. (1990) *Cancer Immunol. Immunother.* **31,** 99–106
16. Anderson, D. H., Harth, G., Horwitz, M. A., and Eisenberg, D. (2001) *J. Mol. Biol.* **307,** 671–681
17. Ohara, N., Matsuo, K., Yamaguchi, R., Yamazaki, A., Tasaka, H., and Yamada, T. (1993) *Infect. Immun.* **61,** 1173–1179
18. Belisle, J. T., Vissa, V. D., Sievert, T., Takayama, K., Brennan, P. J., and Besra, G. S. (1997) *Science* **276,** 1420–1422
19. Hou, J. Y., Graham, J. E., and Clark-Curtiss, J. E. (2002) *Infect. Immun.* **70,** 3714–3726
20. Mariani, F., Cappelli, G., Riccardi, G., and Colizzi, V. (2000) *Gene (Amst.)* **253,** 281–291
21. Matsunaga, I., and Sugita, M. (2007) *Curr. Immunol. Rev.* **3,** 145–150
22. Ulrichs, T., Moody, D. B., Grant, E., Kaufmann, S. H., and Porcelli, S. A. (2003) *Infect. Immun.* **71,** 3076–3087
23. Matsunaga, I., Oka, S., Fujiwara, N., and Yano, I. (1996) *J. Biochem. (Tokyo)* **120,** 663–670

Biochemical and Biophysical Research Communications 377 (2008) 889–893

Contents lists available at ScienceDirect

Biochemical and Biophysical Research Communications

journal homepage: www.elsevier.com/locate/ybbrc

Trans-species activation of human T cells by rhesus macaque CD1b molecules

Daisuke Morita [a,b], Kumiko Katoh [a,b], Toshiyuki Harada [c], Yoshiaki Nakagawa [c], Isamu Matsunaga [a,b], Tomoyuki Miura [d], Akio Adachi [e], Tatsuhiko Igarashi [d,*], Masahiko Sugita [a,b,*]

[a] Laboratory of Cell Regulation, Institute for Virus Research, Kyoto University, 53 Kawahara-cho, Shogoin, Sakyo-ku, Kyoto 606-8507, Japan
[b] Laboratory of Cell Regulation and Molecular Network, Graduate School of Biostudies, Kyoto University, Kyoto 606-8501, Japan
[c] Division of Applied Life Sciences, Graduate School of Agriculture, Kyoto University, Kyoto 606-8502, Japan
[d] Laboratory of Primate Model, Institute for Virus Research, Kyoto University, Kyoto 606-8507, Japan
[e] Department of Virology, Institute of Health Biosciences, The University of Tokushima Graduate School, Tokushima 770-8503, Japan

ARTICLE INFO

Article history:
Received 11 October 2008
Available online 23 October 2008

Keywords:
Rhesus macaque
CD1
Mycobacteria
Glucose monomycolate

ABSTRACT

Despite crucial importance of non-human primates as a model of human infectious diseases, group 1 CD1 genes and proteins have been poorly characterized in these species. Here, we isolated *CD1A*, *CD1B*, and *CD1C* cDNAs from rhesus macaque lymph nodes that encoded full-length CD1 proteins recognized specifically by monoclonal antibodies to human CD1a, CD1b, and CD1c molecules, respectively. The monkey group 1 CD1 isoforms contained amino acid residues and motifs known to be critical for intramolecular disulfide bond formation, N-linked glycosylation, and endosomal trafficking as in human group 1 CD1 molecules. Notably, monkey CD1b molecules were capable of presenting a mycobacterial glycolipid to human CD1b-restricted T cells, providing direct evidence for their antigen presentation function. This also detects for the first time a trans-species crossreaction mediated by group 1 CD1 molecules. Taken together, these results underscore substantial conservation of the group 1 CD1 system between humans and rhesus macaque monkeys.

Besides MHC class I- and II-restricted αβ T cells that recognize protein antigens (Ags), discrete subsets of T cells exist in humans that specifically recognize non-protein Ags in a T-cell receptor (TCR)-dependent manner. These include αβ T cells that recognize lipid, glycolipid, and lipopeptide Ags in the context of group 1 CD1 molecules (CD1a, CD1b, and CD1c) as well as Vγ2⁺Vδ2⁺ γδ T cells that recognize pyrophosphorylated isoprenoid intermediates [1,2]. Both T cell subsets have been implicated in host defense against mycobacterial infection [3], and therefore, animal species that have evolved these T cells in addition to MHC-restricted T cells would serve as an ideal animal model of human tuberculosis. The murine model has long been studied extensively, and by taking advantage of versatile genetic manipulation and a fine array of reagents, many important aspects of host defense against tuberculosis have been demonstrated explicitly, that include a critical role for MHC-restricted T cells [4]. However, a significant difference in pathology has been noted between the two species [3], and the lack of T cells in mice that correspond to human group 1 CD1-resricted T cells and Vγ2⁺Vδ2⁺ γδ T cells makes the animals less useful particularly in an attempt to develop a new chemical class of non-protein vaccines against tuberculosis. In contrast to mice and rats, guinea pigs exhibit pathology that is comparable, if not identical, to that in human tuberculosis, and recent studies have shown that they contain four *CD1B* genes and three *CD1C* genes [5,6]. Nevertheless, CD1a-restricted T cells as well as CD1d-restricted NKT cells may not exist in guinea pigs. These and other significant differences in the organization and function of the immune system between humans and rodents often make it difficult to translate the results obtained from rodent models to humans. Further, certain human pathogens, such as HIV-1, exhibit highly limited host selectivity, and are unable to infect into rodents and other commonly used laboratory animals.

Recently, the value of non-human primates as a model of human infectious diseases has been appreciated greatly for elucidating pathogenesis and for developing vaccines and therapies against microbial infections, such as AIDS and tuberculosis [7,8]. Nevertheless, little has been defined about the genes, proteins, and function of the group 1 CD1 molecules in non-human primates, and therefore, the present study was aimed at identifying the rhesus macaque group 1 CD1 system. We found it highly comparable to that in humans, and rhesus macaque CD1b molecules were indeed able to present a human CD1b-presented mycobacterial glycolipid Ag to specific human T cells.

* Corresponding authors. Fax: +81 75 752 3232 (M. Sugita), +81 75 761 9335 (T. Igarashi).
E-mail addresses: tigarash@virus.kyoto-u.ac.jp (T. Igarashi), msugita@virus.kyoto-u.ac.jp (M. Sugita).

0006-291X/$ - see front matter © 2008 Elsevier Inc. All rights reserved.
doi:10.1016/j.bbrc.2008.10.075

Materials and methods

Isolation of rhesus macaque group 1 CD1 cDNAs. Rhesus monkeys (*Macaca mulatta*) were used in accordance with the institutional regulations approved by the Committee for Experimental Use of Nonhuman Primates of the Institute for Virus Research, Kyoto University, Kyoto, Japan. Total RNA was extracted from rhesus macaque lymph nodes using the RNeasy mini kit (Qiagen, Hilden, Germany), and the first-strand cDNA was synthesized from 0.5 mg of the total RNA using oligo(dT) and PrimeScript reverse transcriptase (Takara Bio, Inc., Otsu, Japan). To amplify specific transcripts, the samples were subjected to PCR amplification with *Pfu* DNA polymerase (Stratagene, La Jolla, CA) for 35 cycles of 30 s at 94 °C, 1 min at 55 °C (for *CD1A*) or 60 °C (for *CD1B* and *CD1C*), 2 min at 72 °C, and a final cycle of 10 min at 72 °C. The primers used were: 5′-GCG GTA CCA AAT AAC ATC TGC AAA TGA C-3′ (sense) and 5′-GCC TCG AGA AGG AGG ATC ATG GTG TAT C-3′ (anti-sense) for *CD1A*; 5′-GCG GTA CCA GTA AGA AGT TGC ATC TCC C -3′ (sense) and 5′-GCC TCG AGG GAG CAG ACA TGG TGA GGG C-3′ (anti-sense) for *CD1B*; 5′-GCG GGT ACC ACC ATG CTG TTT CTG CAG TTT-3′ (sense) and 5′-GCG GCG GCC GCA TTG TAC TAG GCT CCT GG-3′ (anti-sense) for *CD1C*. The PCR products were purified and cloned into pcDNA3.1(+) (Invitrogen, Carlsbad, CA), and DNA sequencing was done in both directions. This procedure was repeated twice to confirm that no PCR-associated errors were introduced.

Transfection. A rhesus macaque kidney epithelial cell line, LLC-MK2 [9], was obtained from ATCC (Manassas, VA). The cells were transfected with pcDNA3.1(+) containing either rhesus macaque *CD1A*, *CD1B*, or *CD1C* by a calcium phosphate precipitation method, using the mammalian transfection kit (Stratagene). The transfected cells were then cultured in DMEM media (Invitrogen) supplemented with 10% fetal calf serum (Hyclone, Logan, UT) and G418 (0.5 mg/ml) (Invitrogen), and the CD1-expressing cells were then enriched by labeling with specific antibodies (Abs), followed by positive selection with magnetic beads coated with goat anti-mouse IgG Abs (Invitrogen). A human lymphoblastoid cell line, T2 [10], was transfected with pCEP4 (Invitrogen) containing *CD1A* or *CD1B* of either human or rhesus macaque origin by electroporation as described [11], followed by selection in RPMI1640 media (Invitrogen) containing 0.2 mg/ml hygromycin B (Invitrogen). A human cervical epithelial cell line, HeLa [12], was transfected with rhesus macaque *CD1C* in pcDNA3.1(+) by a calcium phosphate precipitation method, and selection was performed as described above. These stably transfected cells were used as Ag-presenting cells (APCs) in T cell transfectants stimulation assays.

Flow cytometry. The expression of CD1 proteins on the surface of the LLC-MK2 cell transfectants as well as rhesus macaque thymocytes were analyzed by flow cytometry as described [13,14], using the BD FACSCanto II flow cytometer. The mouse monoclonal Abs (mAbs) used were 10H3 (anti-human CD1a) [15], SN13 (anti-human CD1b) (Ancell, Bayport, MN), M241 (anti-human CD1c) (Ancell), and SP34 (anti-monkey CD3) (BD Biosciences, Franklin Lakes, NJ). MAbs MOPC-31C (BD Biosciences) and RPC5.4 (ATCC) were used as negative controls.

T cell transfectants stimulation assays. TCR-deficient Jurkat cells, J.RT3, reconstituted with either the dideoxymycobactin-specific, CD1a-restricted TCR (J.RT3/CD8-2), the glucose monomycolate (GMM)-specific, CD1b-restricted TCR (J.RT3/LDN5) or the mannosyl phosphomycoketide-specific, CD1c-restricted TCR (J.RT3/CD8-1) have been described previously [16]. The TCR-reconstituted cells (5×10^4/well) were cultured with irradiated APCs expressing a relevant CD1 isoform (1×10^5/well) in wells of 96-well, flat-bottomed microtiter plates (200 μl media/well) in the presence of 10 ng/ml phorbol myristate acetate (PMA) (Sigma, St. Louis, MO) and either the organic extract of *Mycobacterium tuberculosis* H37Ra (for J.RT3/CD8-2 and J.RT3/CD8-1) or *Rhodococcus equi* GMM (for J.RT3/LDN5) at indicated concentrations. After 20 h, aliquots of the culture supernatants were collected, and the amount of interleukin-2 (IL-2) released into the supernatants was measured by the IL-2 ELISA kit (BD Biosciences).

Molecular modeling of rhesus macaque CD1b proteins. Molecular modeling of the rhesus macaque CD1b molecule was performed, using the homology modeling software PDFAMS (Protein Discovery Full Automatic Modeling System; In-Silico Sciences, Inc., Tokyo, Japan) as described [17]. Briefly, the primary sequence of the rhesus macaque CD1b molecule was aligned with the sequence of the human CD1b molecule available from the Protein Data Bank (1UQS), using RPS-BLAST. Amino acid residues differing between the two molecules were mutated, and the obtained 3-dimensional structure was optimized by the simulated annealing method. Subsequently, the molecular model was subjected to energy minimization, using the SYBYL software. The overall structure and the cavity surface of the modeled rhesus macaque CD1b molecule were depicted in association with GMM from *Nocardia farcinica* by utilizing the MOLCAD module of SYBYL.

Results and discussion

Identification of rhesus macaque group 1 CD1 cDNAs

To isolate full-length cDNAs encoding rhesus macaque CD1a and CD1b, the first strand cDNA was synthesized from lymph node total RNA by reverse transcription, and then, PCR was carried out with specific pairs of 5′-end and 3′-end primers that were designed based on the rhesus macaque genomic *CD1A* and *CD1B* sequences. The rhesus macaque genomic *CD1C* sequence was only partially available, and the 3′-end sequence was undermined. Therefore, rhesus macaque *CD1C* cDNA was amplified by PCR using a specific 5′-end primer and a 3′-end primer that was designed based on the sequence of 3′-untranslated region of the human *CD1C* genome. The PCR products thus obtained were of expected size (approximately 1 kb) and the identity of the products was determined by DNA sequences. Identical nucleotide sequences were obtained after two independent PCR amplifications, ruling out the possibility for PCR-associated errors.

Alignment of the deduced amino acid sequences of the putative rhesus macaque *CD1A*, *CD1B*, and *CD1C* genes with the corresponding human CD1 proteins revealed a high-degree homology between the two species (85.6% for CD1a, 94.6% for CD1b, 90.4% for CD1c) (Fig. 1). The cysteine residues (indicated with triangles) involved in the intrachain disulfide bond formation in the α2 and the α3 domains as well as the putative N-linked glycosylation sites (indicated with asterisks) in the α1 and the α2 domains were totally conserved [2]. Further, the cytoplasmic tyrosine-based motif (YXXZ where Y is tyrosine, X is any amino acid, and Z is a hydrophobic amino acid) and its flanking sequences that are known to regulate differential early endosomal and lysosomal trafficking of CD1b and CD1c proteins [12,18,19] were identical between the two species (Fig. 1).

To monitor protein expression of these rhesus macaque *CD1* genes, we first screened mAbs against human CD1 proteins for their cross-reactivity to rhesus macaque thymocytes, a cell type that is presumed to express all forms of group 1 CD1 molecules. As shown in Fig. 2A, mAb clones 10H3 (anti-human CD1a), SN13 (anti-human CD1b), and M241 (anti-human CD1c) labeled a significant fraction of $CD3^{dim}$ thymocytes in a pattern comparable to that for human thymocytes [20]. We then stably transfected each

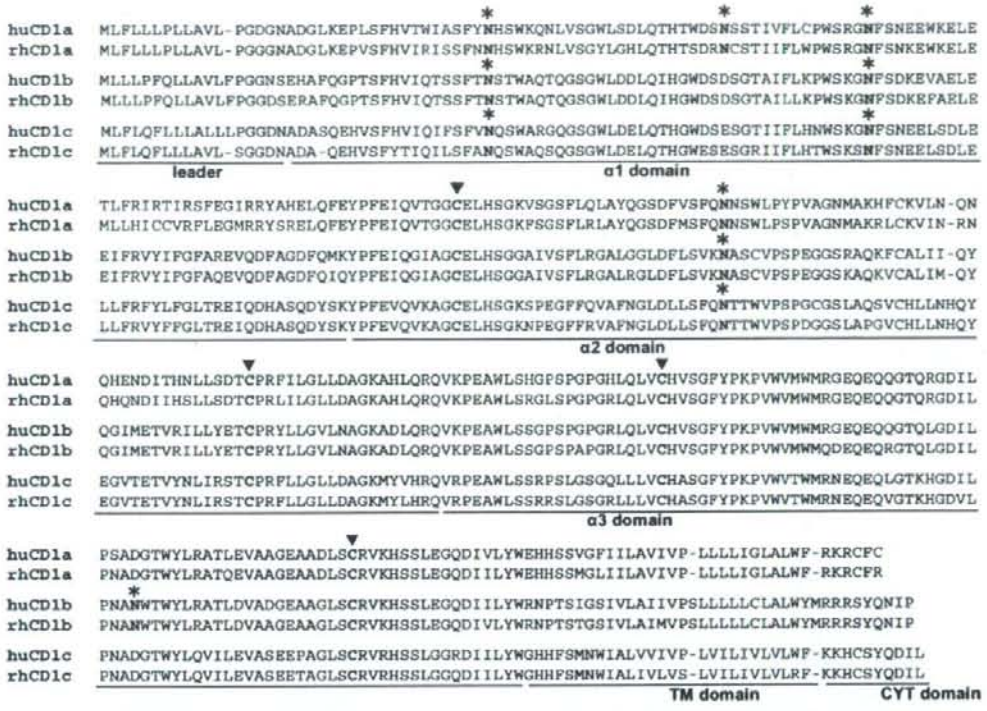

Fig. 1. Alignment of deduced amino acid sequences of human (hu) and rhesus macaque (rh) group 1 CD1 proteins. Residues conserved between the two species are shaded in light gray. Solid triangles denote cysteines conserved in all the group 1 CD1 proteins of both species that are presumed to be involved in intradomain disulfide bond formation. Asterisks indicate potential N-linked glycosylation sites. Dashes represent gaps that have been introduced to maximize alignment. TM domain, transmembrane domain; CYT domain, cytoplasmic domain.

of the putative rhesus macaque *CD1A*, *CD1B*, and *CD1C* genes into a rhesus macaque kidney epithelial cell line, LLC-MK2, and their protein expression was monitored by flow cytometry using the cross-reactive mAbs (Fig. 2B). The 10H3 anti-human CD1a mAb recognized only *CD1A* transfected cells, but not those transfected with the other genes. Similarly, the SN13 anti-human CD1b mAb and the M241 anti-human CD1c mAb showed specific reactivity to cells transfected with the *CD1B* and the *CD1C* genes, respectively. These results provided both evidence for protein expression of the isolated genes and further support for their identity, and therefore, the nucleotide sequences of the putative *CD1A*, *CD1B*, and *CD1C* cDNAs were deposited to the DDBJ/GenBank/EMBL databases as those of rhesus macaque *CD1A* (Accession Nos: AB458511), *CD1B* (AB458512), and *CD1C* (AB458513), respectively.

Trans-species activation of human T cells by rhesus macaque CD1b molecules

With the exception of mice and rats, group 1 CD1 genes have been identified in virtually all mammalian animals so far analyzed, but the Ag presentation function of their products has not been demonstrated so explicitly as in humans [21]. This is partly due to difficulties in obtaining specific T cell lines and clones that recognize lipid Ags in the context of CD1 molecules of a given animal species. Because of the highly conserved amino acid sequences of human and rhesus macaque group 1 CD1 proteins, we considered the possibility that rhesus macaque CD1 molecules might bind lipid Ags that were known to be presented by human CD1 molecules, and interact with specific human TCRs. To address this, human TCRs derived either from a dideoxymycobactin-specific, CD1a-restricted T cell line (CD8-2), from a GMM-specific, CD1b-restricted T cell line (LDN5) or from a mannosyl phosphomycoketide-specific, CD1c-restricted T cell line (CD8-1) were reconstituted in TCR-deficient Jurkat cells (J.RT3) by gene transfer, and the T cell reactivity to specific Ag in the presence of cell transfectants expressing a relevant CD1 isoform of either human or rhesus macaque origin was assessed by measuring IL-2 released from the T cells. J.RT3/CD8-2 cells responded to dideoxymycobactin in the presence of APCs expressing human CD1a molecules, but not those expressing rhesus macaque CD1a molecules (Fig. 3, top panel). Similarly, J.RT3/CD8-1 cells responded to mannosyl phosphomycoketide in the presence of APCs expressing human CD1c molecules, but not those expressing rhesus macaque CD1c molecules (bottom panel). Strikingly, however, APCs expressing rhesus macaque CD1b molecules were capable of presenting GMM efficiently to J.RT3/LDN5 cells (middle panel), providing evidence for their Ag presentation function. The apparently more efficient Ag presentation function for rhesus macaque CD1b molecules as compared with human CD1b molecules could be accounted for by the slightly higher expression on rhesus macaque CD1b transfectants than on human CD1b transfectants (data not shown).

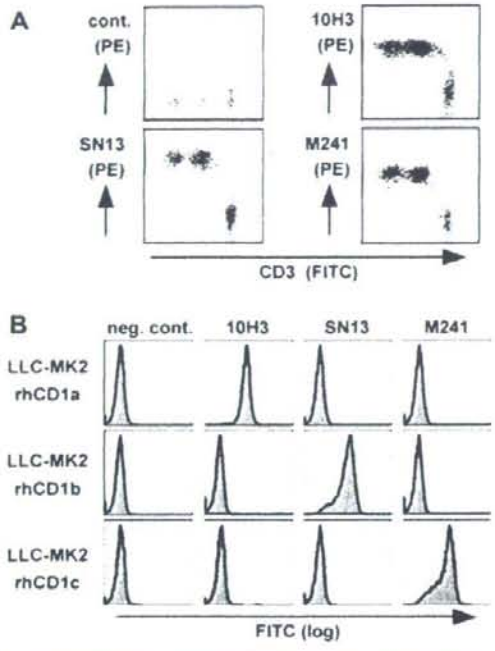

Fig. 2. Cross-reactivity of anti-human CD1 mAbs to rhesus macaque group 1 CD1 proteins. (A) Rhesus macaque thymocytes were double-labeled with the SP34 anti-CD3 mAb and either the 10H3 anti-human CD1a mAb, the SN13 anti-human CD1b mAb, the M241 anti-human CD1c mAb, or negative control Abs, followed by analysis by flow cytometry. (B) A rhesus macaque kidney cell line, LLC-MK2, that stably transfected with either rhesus macaque *CD1A* (LLC-MK2 rhCD1a), *CD1B* (LLC-MK2 rhCD1b), or *CD1C* (LLC-MK2 rhCD1c) were labeled with indicated mAbs and analyzed by flow cytometry.

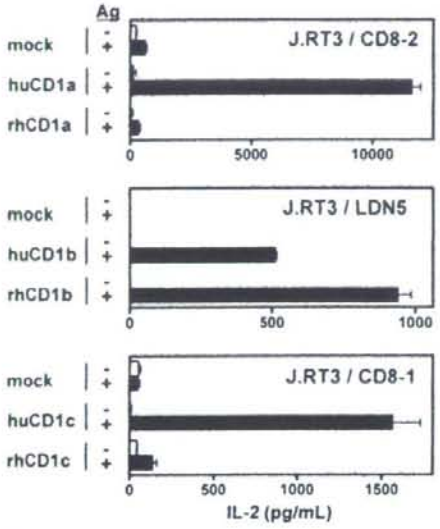

Fig. 3. Ag presentation function of rhesus macaque CD1b molecules. The J.RT3/CD8-2 cells were cultured in the presence or absence of the organic extract of *M. tuberculosis* (50 mg/ml) with T2 cells expressing either human CD1a (huCD1a) or rhesus macaque CD1a (rhCD1a) or those that were mock-transfected (top panel). The J.RT3/LDN5 cells were cultured in the presence or absence of purified GMM (5 mg/ml) with T2 cells expressing either human CD1b (huCD1b) or rhesus macaque CD1b (rhCD1b) or those that were mock transfected (middle panel). The J.RT3/CD8-1 cells were cultured in the presence or absence of the organic extract of *M. tuberculosis* (1.56 mg/ml) with HeLa cells expressing either human CD1c (huCD1c) or rhesus macaque CD1c (rhCD1c) or those that were mock transfected (bottom panel). After 20 h, the culture supernatants were harvested and the amount of IL-2 secreted into the supernatants were measured.

Trans-species crossreaction has never been observed previously for any of the group 1 CD1 molecules. Nevertheless, a molecular model of the rhesus macaque CD1b molecule has detected the α1 and α2 helix structure as well as intramolecular pockets (A′, C′, and F′) and a tunnel (T′) virtually identical to those for human CD1b molecules [22,23], allowing stable interaction with a human CD1b-presented mycobacterial Ag, GMM (Fig. 4). Further, amino acid residues, such as E80 and D83 in the α1 domain and T157 and T165 in the α2 domain, that are proposed to be critical for interaction with specific TCRs [24] are shared between rhesus macaque and human CD1b molecules, suggesting a conserved function for CD1b in these two species. The extent of amino acid sequence conservation is higher in CD1b than in CD1a and CD1c (Fig. 1), which may imply that immune responses to mycolic acid-containing glycolipds are critical for host defense against tuberculosis. So far, no experimental animals have proved extremely useful as a model for studying the group 1 CD1-mediated immunity in human infectious diseases. The present study underscores that monkeys are indispensable for a variety of challenges, including development of a new type of lipid-based vaccines against tuberculosis.

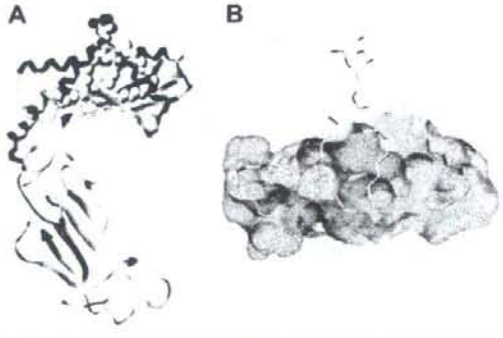

Fig. 4. A molecular model of rhesus macaque CD1b proteins. The rhesus macaque CD1b structure was constructed, based on the crystal structure of the human CD1b-GMM complex. (A) The overall structure of the rhesus macaque CD1b-GMM complex is shown, in which the CD1b heavy chain is depicted in ribbon diagram and the non-hydrogen atoms of GMM are drawn as van der Waals spheres (carbon in gray; oxygen in red). The associated β2-microglobulin is not depicted for simplicity purposes. (B) The binding surface of the Ag-binding groove is drawn in green with the bound GMM in stick (carbon in gray; oxygen in red). (For interpretation of the references to colour in this figure legend, the reader is referred to the web version of this paper).

Acknowledgments

We thank Drs. M. Brenner, D. Olive, and C. Mawas for their gifts of reagents. This work was supported by grants from the Ministry of Education, Culture, Sports, Science and Technology (Grant-in-Aid from Scientific Research on Priority Areas), from the Japan Society for the Promotion of Science (Grant-in-Aid for Scientific Research

(B)), and from the Ministry of Health, Labour, and Welfare (Research on Emerging and Re-emerging infectious Diseases) (to M.S.).

References

[1] C.T. Morita, R.A. Mariuzza, M.B. Brenner, Antigen recognition by human gamma delta T cells: pattern recognition by the adaptive immune system, Springer Semin. Immunopathol. 22 (2000) 191–217.
[2] S.A. Porcelli, The CD1 family: a third lineage of antigen-presenting molecules, Adv. Immunol. 59 (1995) 1–98.
[3] R.J. North, Y.J. Jung, Immunity to tuberculosis, Annu. Rev. Immunol. 22 (2004) 599–623.
[4] T. Mogues, M.E. Goodrich, L. Ryan, R. LaCourse, R.J. North, The relative importance of T cell subsets in immunity and immunopathology of airborne *Mycobacterium tuberculosis* infection in mice, J. Exp. Med. 193 (2001) 271–280.
[5] C.C. Dascher, K. Hiromatsu, J.W. Naylor, P.P. Brauer, K.A. Brown, J.R. Storey, S.M. Behar, E.S. Kawasaki, S.A. Porcelli, M.B. Brenner, K.P. LeClair, Conservation of a CD1 multigene family in the guinea pig, J. Immunol. 163 (1999) 5478–5488.
[6] K. Hiromatsu, C.C. Dascher, M. Sugita, C. Gingrich-Baker, S.M. Behar, K.P. LeClair, M.B. Brenner, S.A. Porcelli, Characterization of guinea-pig group 1 CD1 proteins, Immunology 106 (2002) 159–172.
[7] D.H. Barouch, J. Kunstman, M.J. Kuroda, J.E. Schmitz, S. Santra, F.W. Peyerl, G.R. Krivulka, K. Beaudry, M.A. Lifton, D.A. Gorgone, D.C. Montefiori, M.G. Lewis, S.M. Wolinsky, N.L. Letvin, Eventual AIDS vaccine failure in a rhesus monkey by viral escape from cytotoxic T lymphocytes, Nature 415 (2002) 335–339.
[8] Y. Shen, D. Zhou, L. Qiu, X. Lai, M. Simon, L. Shen, Z. Kou, Q. Wang, L. Jiang, J. Estep, R. Hunt, M. Clagett, P.K. Sehgal, Y. Li, X. Zeng, C.T. Morita, M.B. Brenner, N.L. Letvin, Z.W. Chen, Adaptive immune response of Vgamma2Vdelta2+ T cells during mycobacterial infections, Science 295 (2002) 2255–2258.
[9] R.N. Hull, W.R. Cherry, O.J. Tritch, Growth characteristics of monkey kidney cell strains LLC-MK1, LLC-MK2, and LLC-MK2(NCTC-3196) and their utility in virus research, J. Exp. Med. 115 (1962) 903–918.
[10] M.L. Wei, P. Cresswell, HLA-A2 molecules in an antigen-processing mutant cell contain signal sequence-derived peptides, Nature 356 (1992) 443–446.
[11] M. Sugita, E.P. Grant, E. van Donselaar, V.W. Hsu, R.A. Rogers, P.J. Peters, M.B. Brenner, Separate pathways for antigen presentation by CD1 molecules, Immunity 11 (1999) 743–752.
[12] M. Sugita, X. Cao, G.F. Watts, R.A. Rogers, J.S. Bonifacino, M.B. Brenner, Failure of trafficking and antigen presentation by CD1 in AP-3-deficient cells, Immunity 16 (2002) 697–706.
[13] M. Cernadas, M. Sugita, N. van der Wel, X. Cao, J.E. Gumperz, S. Maltsev, G.S. Besra, S.M. Behar, P.J. Peters, M.B. Brenner, Lysosomal localization of murine CD1d mediated by AP-3 is necessary for NK T cell development, J. Immunol. 171 (2003) 4149–4155.
[14] H. Suzuki, M. Motohara, A. Miyake, K. Ibuki, Y. Fukazawa, K. Inaba, K. Masuda, N. Minato, H. Kawamoto, M. Hayami, T. Miura, Intrathymic effect of acute pathogenic SHIV infection on T-lineage cells in newborn macaques, Microbiol. Immunol. 49 (2005) 667–679.
[15] D. Olive, P. Dubreuil, C. Mawas, Two distinct TL-like molecular subsets defined by monoclonal antibodies on the surface of human thymocytes with different expression on leukemia lines, Immunogenetics 20 (1984) 253–264.
[16] E.P. Grant, M. Degano, J.P. Rosat, S. Stenger, R.L. Modlin, I.A. Wilson, S.A. Porcelli, M.B. Brenner, Molecular recognition of lipid antigens by T cell receptors, J. Exp. Med. 189 (1999) 195–205.
[17] C.E. Wheelock, Y. Nakagawa, T. Harada, N. Oikawa, M. Akamatsu, G. Smagghe, D. Stefanou, K. Iatrou, L. Swevers, High-throughput screening of ecdysone agonists using a reporter gene assay followed by 3-D QSAR analysis of the molting hormonal activity, Bioorg. Med. Chem. 14 (2006) 1143–1159.
[18] M. Sugita, R.M. Jackman, E. van Donselaar, S.M. Behar, R.A. Rogers, P.J. Peters, M.B. Brenner, S.A. Porcelli, Cytoplasmic tail-dependent localization of CD1b antigen-presenting molecules to MIICs, Science 273 (1996) 349–352.
[19] M. Sugita, N. Van Der Wel, R.A. Rogers, P.J. Peters, M.B. Brenner, CD1c molecules broadly survey the endocytic system, Proc. Natl. Acad. Sci. USA 97 (2000) 8445–8450.
[20] L.L. Lanier, J.P. Allison, J.H. Phillips, Correlation of cell surface antigen expression on human thymocytes by multi-color flow cytometric analysis: implications for differentiation, J. Immunol. 137 (1986) 2501–2507.
[21] K. Hiromatsu, C.C. Dascher, K.P. LeClair, M. Sugita, S.T. Furlong, M.B. Brenner, S.A. Porcelli, Induction of CD1-restricted immune responses in guinea pigs by immunization with mycobacterial lipid antigens, J. Immunol. 169 (2002) 330–339.
[22] T. Batuwangala, D. Shepherd, S.D. Gadola, K.J. Gibson, N.R. Zaccai, A.R. Fersht, G.S. Besra, V. Cerundolo, E.Y. Jones, The crystal structure of human CD1b with a bound bacterial glycolipid, J. Immunol. 172 (2004) 2382–2388.
[23] S.D. Gadola, N.R. Zaccai, K. Harlos, D. Shepherd, J.C. Castro-Palomino, G. Ritter, R.R. Schmidt, E.Y. Jones, V. Cerundolo, Structure of human CD1b with bound ligands at 2.3 A, a maze for alkyl chains, Nat. Immunol. 3 (2002) 721–726.
[24] A. Melian, G.F. Watts, A. Shamshiev, G. De Libero, A. Clatworthy, M. Vincent, M.B. Brenner, S. Behar, K. Niazi, R.L. Modlin, S. Almo, D. Ostrov, S.G. Nathenson, S.A. Porcelli, Molecular recognition of human CD1b antigen complexes: evidence for a common pattern of interaction with alpha beta TCRs, J. Immunol. 165 (2000) 4494–4504.

JOURNAL OF BACTERIOLOGY, Dec. 2008, p. 7918–7924 Vol. 190, No. 24
0021-9193/08/$08.00+0 doi:10.1128/JB.00911-08

The *Mycobacterium avium* Complex *gtfTB* Gene Encodes a Glucosyltransferase Required for the Biosynthesis of Serovar 8-Specific Glycopeptidolipid[▽]

Yuji Miyamoto,[1]* Tetsu Mukai,[1] Yumi Maeda,[1] Masanori Kai,[1] Takashi Naka,[2] Ikuya Yano,[2] and Masahiko Makino[1]

Department of Microbiology, Leprosy Research Center, National Institute of Infectious Diseases, 4-2-1 Aobacho, Higashimurayama, Tokyo 189-0002, Japan,[1] and Japan BCG Central Laboratory, 3-1-5 Matsuyama, Kiyose, Tokyo 204-0022, Japan[2]

Received 2 July 2008/Accepted 29 September 2008

***Mycobacterium avium* complex (MAC) is one of the most common opportunistic pathogens widely distributed in the natural environment. The 28 serovars of MAC are defined by variable oligosaccharide portions of glycopeptidolipids (GPLs) that are abundant on the surface of the cell envelope. These GPLs are also known to contribute to the virulence of MAC. Serovar 8 is one of the dominant serovars isolated from AIDS patients, but the biosynthesis of serovar 8-specific GPL remains unknown. To clarify this, we compared gene clusters involved in the biosynthesis of several serovar-specific GPLs and identified the genomic region predicted to be responsible for GPL biosynthesis in a serovar 8 strain. Sequencing of this region revealed the presence of four open reading frames, three unnamed genes and *gtfTB*, the function of which has not been elucidated. The simultaneous expression of *gtfTB* and two downstream genes in a recombinant *Mycobacterium smegmatis* strain genetically modified to produce serovar 1-specific GPL resulted in the appearance of 4,6-*O*-(1-carboxyethylidene)-3-*O*-methyl-glucose, which is unique to serovar 8-specific GPL, suggesting that these three genes participate in its biosynthesis. Furthermore, functional analyses of *gtfTB* indicated that it encodes a glucosyltransferase that transfers a glucose residue via 1→3 linkage to a rhamnose residue of serovar 1-specific GPL, which is critical to the formation of the oligosaccharide portion of serovar 8-specific GPL. Our findings might provide a clue to understanding the biosynthetic regulation that modulates the biological functions of GPLs in MAC.**

Mycobacteria are pathogens that cause diseases such as tuberculosis and leprosy. In addition, nontuberculous mycobacteria, which are widely distributed in the natural environment, cause opportunistic pulmonary infections resembling tuberculosis. These mycobacteria are distinguished by a multilayered cell envelope consisting of peptidoglycan, mycolyl arabinogalactan, and surface glycolipids (9, 13). The surface glycolipids are abundant and structurally different, and they may act as a barrier to immune responses (9, 13). Glycopeptidolipids (GPLs) are major glycolipid components present on the surface of several species of nontuberculous mycobacteria (40). All of these GPLs have a conserved core structure that is composed of a fatty acyl tetrapeptide glycosylated with 6-deoxytalose (6-d-Tal) and *O*-methyl-rhamnose (O-Me-Rha) and are termed non-serovar-specific GPLs (nsGPLs) (2, 4, 14). On the other hand, the GPLs of *Mycobacterium avium* complex (MAC), nontuberculous mycobacteria consisting principally of two species, *M. avium* and *M. intracellulare*, have various haptenic oligosaccharides linked to the 6-d-Tal residue of nsGPLs, resulting in serovar-specific GPLs (ssGPLs) (2, 4, 40). The oligosaccharide portions of ssGPLs define MAC serovars that are classified into 28 types. The serovar 1-specific GPL, with Rha linked to the 6-d-Tal residue, is the basic oligosaccharide unit of all ssGPLs (11). The Rha residue of serovar 1-specific GPL is further extended by various glycosylation steps, such as rhamnosylation, fucosylation, and glucosylation (11). These glycosylation steps generate structural diversity in GPLs of MAC (11). However, because of their complexity, most of the biosynthetic pathways for ssGPLs have not been fully determined. We recently showed that the biosynthesis of nsGPLs was regulated by a combination of glycosyltransferases (31). Therefore, each glycosyltransferase might mediate a specific step in the biosynthesis of ssGPLs.

In terms of biological activity, it has been reported that the properties of ssGPLs are notably different from each other and that some of the properties play a role in affecting host responses to MAC infections (3, 5, 21, 27, 37, 38). Moreover, epidemiological studies have shown that serovars 1, 4, and 8 are distributed predominantly in North America and are also frequently isolated from AIDS patients (24, 39, 41). However, in contrast to other ssGPLs, the serovar 8-specific GPL is reported to be able to induce altered immune responses (3, 21). The biosynthetic pathway for serovar 8-specific GPL, particularly its oligosaccharide portion that includes a unique 4,6-*O*-(1-carboxyethylidene)-3-*O*-methyl-glucose (Glc) residue (7, 8) that may determine the specificity of serovar 8, remains unknown (Table 1). In this study, we investigated the genomic region assumed to be associated with the biosynthesis of GPL in MAC serovar 8 strain and identified the genes involved in

* Corresponding author. Mailing address: Department of Microbiology, Leprosy Research Center, National Institute of Infectious Diseases, 4-2-1 Aobacho, Higashimurayama, Tokyo 189-0002, Japan. Phone: 81-42-391-8211. Fax: 81-42-394-9092. E-mail: yujim@nih.go.jp.
▽ Published ahead of print on 10 October 2008.

TABLE 1. Oligosaccharide structures of serovar 1- and 8-specific GPLs

Serovar	Oligosaccharide	Reference(s)
1	α-L-Rha-(1→2)-L-6-d-Tal	17
8	4,6-*O*-(1-carboxyethylidene)-3-*O*-methyl-β-D-Glc-(1→3)-α-L-Rha-(1→2)-L-6-d-Tal	7, 8

the glycosylation pathway leading to the formation of serovar 8-specific GPL.

MATERIALS AND METHODS

Bacterial strains, culture conditions, and DNA manipulation. Table 2 shows the bacterial strains and vectors used in this study. MAC strains were grown in Middlebrook 7H9 broth (Difco) with 0.05% Tween 80 supplemented with 10% Middlebrook ADC enrichment (BBL). Recombinant *M. smegmatis* strains used for GPL production were cultured in Luria-Bertani broth with 0.2% Tween 80. Isolation of DNA and transformation of *M. smegmatis* strains were performed as previously described (32). The genomic regions of MAC strains were amplified by a two-step PCR using TaKaRa *LA Taq* with GC buffer and the following program: denaturation at 98°C for 20 s and annealing-extension at 68°C for an appropriate time depending on the length of the targeted region. *Escherichia coli* strain DH5α was used for routine manipulation and propagation of plasmid DNA. When necessary, antibiotics were added as follows: kanamycin, 50 μg/ml for *E. coli* and 25 μg/ml for *M. smegmatis*; and hygromycin B, 150 μg/ml for *E. coli* and 75 μg/ml for *M. smegmatis*. Oligonucleotide primers used in this study are listed in Table 3.

Construction of expression vectors. The *rtfA* gene was amplified from genomic DNA of *M. avium* strain JATA51-01 using primers RTFA-S and RTFA-A. The PCR products were digested with each restriction enzyme and cloned into the BamHI-PstI site of pMV261 to obtain pMV-rtfA. To use the site-specific integrating mycobacterial vector more conveniently, we constructed pYM301a containing an AflII site in pYM301. The region encompassing *gtfTB*, ORF3, and ORF4 was amplified from genomic DNA of MAC serovar 8 strain ATCC 35771 using primers GTFTB-S and ORF4-A. In addition, *gtfTB* was amplified using primers GTFTB-S and GTFTB-A. The PCR products were digested with each restriction enzyme and cloned into the PstI-EcoRI site of pYM301a to obtain pYM-gtfTB-orf3-orf4 and pYM-gtfTB (Table 2).

Isolation and purification of GPLs. Harvested bacterial cells were allowed to stand in $CHCl_3$-CH_3OH (2:1, vol/vol) for several hours at room temperature. After water was added, total-lipid extracts were obtained from the organic phase and evaporated to dryness. Total-lipid extracts were subjected to mild alkaline hydrolysis as previously described (32, 33) to obtain crude GPL extracts. For analytical thin-layer chromatography (TLC), crude GPLs obtained from the same wet weight of harvested bacterial cells were spotted on Silica Gel 60 plates (Merck) using $CHCl_3$-CH_3OH-H_2O (30:8:1, vol/vol/vol) as the solvent and were visualized by spraying the plates with 10% H_2SO_4 and charring. Purified GPLs were prepared from crude GPLs by preparative TLC on the same plates, and each GPL was extracted from the corresponding band. Perdeuteriomethylation was carried out as previously described (6, 12, 17).

TABLE 3. Oligonucleotide primers used in this study

Primer	Sequence[a]	Restriction site
RTFA-S	5′-CGGGATCCCATGAAATTTGCTGTGGCAAG-3′	BamHI
RTFA-A	5′-AACTGCAGCTCAGCGACTTCGCTGCGCTTC-3′	PstI
GTFTB-S	5′-AACTGCAGAAATGACCGCCACAACCAGGGC-3′	PstI
GTFTB-A	5′-GGAATTCTCAGGCGCTCAGTGGCTCGTC-3′	EcoRI
ORF4-A	5′-GGAATTCCTAGGGCGCCAATTCGATGAG-3′	EcoRI
GTFB-U4	5′-GGAATTCGGTCGACTCGACGAAGCCGAC-3′	EcoRI
DRRC-A	5′-GGAATTCTGCAGGCGGGGCGACTCCTGCT-3′	EcoRI

[a] Underlining indicates restriction sites.

GC-MS and MALDI-TOF MS analysis. Crude and purified GPLs were hydrolyzed in 2 M trifluoroacetic acid (2 h, 120°C), and the released sugars were reduced with $NaBD_4$ and then acetylated with pyridine-acetic anhydride (1:1, vol/vol) at room temperature overnight. The resulting alditol acetates were separated and analyzed by gas chromatography-mass spectrometry (GC-MS) with a TRACE DSQ (Thermo Electron) equipped with an SP-2380 column (Supelco) using helium gas. The following program was used: temperature increased from 52 to 172°C at a rate of 40°C/min and then increased from 172 to 250°C at a rate of 3°C/min. To determine the total mass of the purified GPLs, matrix-assisted laser desorption ionization—time of flight (MALDI-TOF) mass spectra (in the positive mode) were obtained with a QSTAR XL (Applied Biosystems) using a pulse laser with emission at 337 nm. Samples mixed with 2,5-dihydroxybenzoic acid as the matrix were analyzed in the reflectron mode with an accelerating voltage of 20 kV and with operation in positive ion mode.

Nucleotide sequence accession number. The 4.6-kb genomic region amplified from MAC serovar 8 strain ATCC 35771 using primers GTFB-U4 and DRRC-A has been deposited in the DDBJ nucleotide sequence database under accession number AB437139.

RESULTS

Isolation and sequencing of the 4.6-kb genomic region responsible for GPL biosynthesis in MAC serovar 8. Lacking information on the genes responsible for biosynthesis of serovar 8-specific GPL, we compared and analyzed the genomic regions likely to be responsible for GPL biosynthesis in several

TABLE 2. Bacterial strains and vectors used in this study

Strain or vector	Characteristics	Source or reference
Bacteria		
E. coli DH5α	Cloning host	TaKaRa
M. smegmatis mc^{2}155	Expression host	35
M. intracellulare ATCC 35771	MAC serovar 8 strain	29
M. avium JATA51-01	Source of *rtfA*	17
Vectors		
pYM301	Source of pYM301a	30
pYM301a	Site-specific integrating mycobacterial vector carrying an *hsp60* promoter cassette and AflII site	This study
pMV261	*E. coli-Mycobacterium* shuttle vector carrying an *hsp60* promoter cassette	36
pMV-rtfA	pMV261 with *rtfA*	This study
pYM-gtfTB	pYM301a with *gtfTB*	This study
pYM-gtfTB-orf3-orf4	pYM301a with *gtfTB*, ORF3, and ORF4	This study

FIG. 1. Organization of the 4.6-kb genomic region isolated from MAC serovar 8 strain. Filled triangles indicate the primers used for PCR amplification.

MAC serovars (16, 28). Most of these regions have high homology to each other, while the segment between the *gtfB* and *drrC* genes was found to vary in the strains. Therefore, we assumed that this segment contains genes involved in the formation of the unique Glc residue in serovar 8-specific GPL. To clone the *gtfB-drrC* region by using PCR, we designed various primers containing sequences derived from other MAC strains. By examining combinations of several pairs of primers, a 4.6-kb fragment was amplified from genomic DNA of a MAC serovar 8 strain when primers GTFB-U4 and DRRC-A were used (Fig. 1). Sequencing of this 4.6-kb fragment revealed four complete open reading frames (Fig. 1). The deduced amino acid sequences encoded by ORF1, ORF2, ORF3, and ORF4 were found to be identical to the amino acid sequences of four functionally undefined proteins from *M. avium* strain 104, MAV_3253, MAV_3255, MAV_3256, and MAV_3257, respectively (GenBank accession no. NC_008595.1). *M. avium* strain A5 also possessed a genomic region harboring ORF2, ORF3, and ORF4 (GenBank accession no. AY130970.1). These four open reading frames are predicted to encode the following proteins: ORF1, a putative glycosyltransferase similar to GtfD, which has been identified as a fucosyltransferase involved in the biosynthesis of serovar 2-specific GPL (73% identity) (30); ORF2, a putative glycosyltransferase, designated GtfTB, showing high homology to Rv1516c of *M. tuberculosis* (61% identity) (28); ORF3, a putative polysaccharide pyruvyltransferase similar to MSMEG_4736 and MSMEG_4737 of *M. smegmatis* (61 and 58% identity, respectively) (GenBank accession no. NC_008596.1); and ORF4, a putative *O*-methyltransferase similar to MSMEG_4739 of *M. smegmatis* (55% identity) (GenBank accession no. NC_008596.1).

Identification of the genes required for synthesis of the sugar residue unique to serovar 8-specific GPL. Based on the deduced functions of the genes in the 4.6-kb fragment, we focused on *gtfTB* (ORF2), ORF3, and ORF4 and characterized them by performing expression analyses. Because the serovar 8-specific GPL has a structure in which the Rha residue of serovar 1-specific GPL is further glycosylated (Table 1), it was necessary to prepare a strain producing serovar 1-specific GPL that could be the substrate for the enzymes participating in the biosynthesis of serovar 8-specific GPL. For this, as previously demonstrated, we created a recombinant *M. smegmatis* strain, designated MS-S1, by introducing the plasmid vector pMV-rtfA having the *M. avium rtfA* gene, which converts nsGPLs to serovar 1-specific GPL (30). We then introduced the integrative expression vector pYM-gtfTB possessing *gtfTB* into MS-S1 and assessed GPL profiles by performing a TLC analysis (Fig. 2). By comparison with the profile of MS-S1/pYM301a (vector control) (Fig. 2, lane A), two new spots, designated spots GPL-SG-U and -D, were observed in MS-S1/pYM-gtfTB (Fig. 2, lane B), indicating that serovar 1-specific

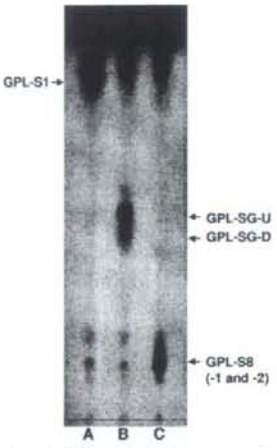

FIG. 2. TLC of crude GPL extracts from recombinant *M. smegmatis* strains MS-S1/pYM301a (A), MS-S1/pYM-gtfTB (B), and MS-S1/pYM-gtfTB-orf3-orf4 (C). GPL extracts were prepared from the total-lipid fraction, and this was followed by mild alkaline hydrolysis. Samples were spotted and developed using $CHCl_3$-CH_3OH-H_2O (30:8:1, vol/vol/vol).

GPL was converted to structurally different compounds by expression of *gtfTB*. Moreover, when the expression vector pYM-gtfTB-orf3-orf4 containing *gtfTB*, ORF3, and ORF4 was introduced into MS-S1, another new spot, designated GPL-S8, appeared (Fig. 2, lane C), implying that the structure of GPL-SG-U and -D was further modified by the products of ORF3 and ORF4. To confirm that these compounds contain the sugar residues associated with serovar 8-specific GPL, we performed a GC-MS analysis of the monosaccharides released from crude GPL extracts of each recombinant strain and the MAC serovar 8 strain (Fig. 3). The results showed that there was an excess of Glc, together with Rha, 6-d-Tal, 3,4-di-*O*-methyl-Rha, and 2,3,4-tri-*O*-methyl-Rha, in the profile of MS-S1/pYM-gtfTB compared with other profiles, as well as minor Glc peaks presumably derived from traces of trehalose-containing glycolipids (Fig. 3B). This indicates that the *gtfTB* gene mediates the transfer of a Glc residue to serovar 1-specific GPL. In contrast, the profile of MS-S1/pYM-gtfTB-orf3-orf4 revealed the presence of 4,6-*O*-(1-carboxyethylidene)-3-*O*-methyl-Glc, which was also detected in the MAC serovar 8 strain (Fig. 3C and D), demonstrating that the three genes are associated with the formation of the unique sugar residue of serovar 8-specific GPL.

Functional characterization of *gtfTB*. Expression analysis showed that serovar 1-specific GPL was converted to new compounds containing Glc when the *gtfTB* gene was expressed (Fig. 2, lane B, and Fig. 3B). Although these results suggested that the product of *gtfTB* participates in the formation of a Glc residue, it is not clear whether *gtfTB* encodes the glycosyltransferase that transfers Glc via 1→3 linkage to the Rha residue of serovar 1-specific GPL, whose linkage was previously detected in serovar 8-specific GPL (7, 8). To elucidate the function of *gtfTB*, we determined the linkage of sugar moieties of GPL-SG-U and -D, which were produced by recombinant strain

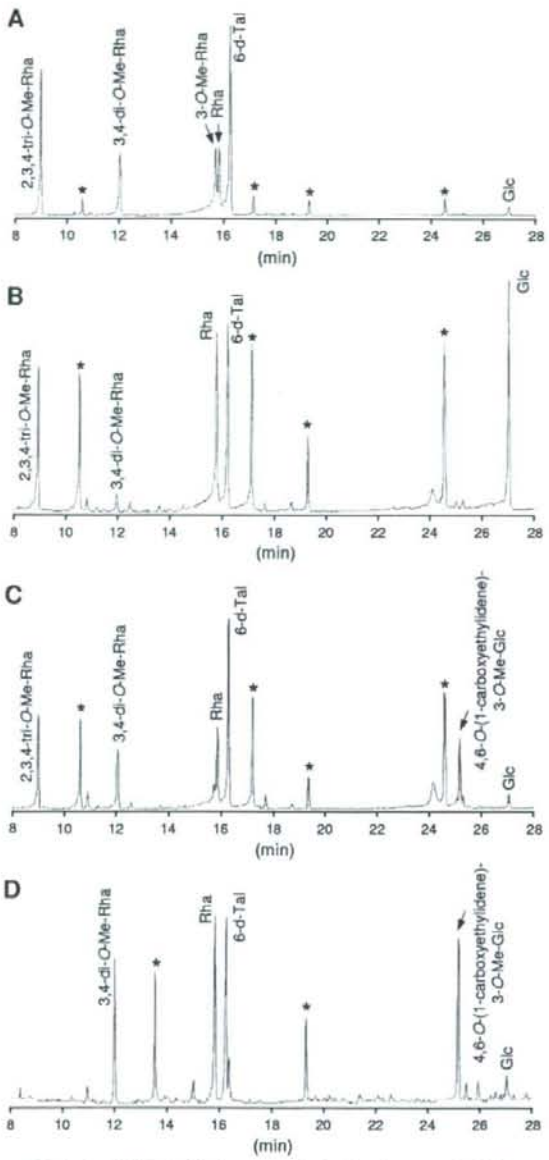

FIG. 3. GC-MS of alditol acetate derivatives from crude GPL extracts of recombinant strains *M. smegmatis* MS-S1/pYM301a (A), MS-S1/pYM-gtfTB (B), and MS-S1/pYM-gtfTB-orf3-orf4 (C) and a MAC serovar 8 strain (D). GPL extracts were prepared from the total-lipid fraction, and this was followed by mild alkaline hydrolysis. Asterisks indicate noncarbohydrates. Me, methyl.

MS-S1/pYM-gtfTB (Fig. 2, lane B). After extraction of the products from the corresponding bands on the TLC plate, purified GPL-SG-U and -D were subjected to perdeuteriomethylation followed by GC-MS. The differences in the TLC profiles of GPL-SG-U and -D might have been due to the presence or absence of fatty acid methylation, which is often observed in *M. smegmatis* GPLs (23, 31), whereas the GC-MS profiles and fragmentation ions for GPL-SG-U and -D were identical, demonstrating that GPL-SG-U and -D had the same sugar moieties and linkages. Therefore, the profiles of GPL-SG-U shown here are representative of GPL-SG-U and -D. The GC-MS profile of GPL-SG-U contained four peaks corresponding to 6-d-Tal, Rha, Glc, and 2,3,4-tri-*O*-methyl-Rha (data not shown). The characteristic spectra for Glc, Rha, and 6-d-Tal are shown in Fig. 4. The spectrum of Glc had fragment ions at *m/z* 121, 167, and 168, which represent the presence of deuteriomethyl groups at positions C-2, C-3, and C-4 (Fig. 4A). In contrast, fragment ions at *m/z* 121, 134, 193, and 240 were detected for Rha, indicating that a deuteriomethyl group was introduced at positions C-2 and C-4 of Rha, in which position C-3 was acetylated (Fig. 4B). In addition, detection of fragment ions at *m/z* 134, 181, and 193 (Fig. 4C) revealed that there was deuteriomethylation at positions C-3 and C-4 in 6-d-Tal. These results demonstrated that position C-1 of Glc is linked to position C-3 of Rha but not to position C-2 of 6-d-Tal, because it has been determined previously that position C-1 of Rha is linked to position C-2 of 6-d-Tal in the oligosaccharide of serovar 1-specific GPL (17). Accordingly, the oligosaccharide structures of GPL-SG-U and -D were determined to have Glc-(1→3)-Rha-(1→2)-6-d-Tal at D-*allo*-Thr, demonstrating that *gtfTB* encodes the glucosyltransferase that transfers a Glc residue via 1→3 linkage to the Rha residue of serovar 1-specific GPL.

Structural assignment of GPL-S8 synthesized by expression of *gtfTB*, ORF3, and ORF4. GC-MS of the crude GPL extract from MS-S1/pYM-gtfTB-orf3-orf4 revealed the presence of 4,6-*O*-(1-carboxyethylidene)-3-*O*-methyl-Glc (Fig. 3C). To confirm that this structural component was derived from GPL-S8, we performed GC-MS and MALDI-TOF MS analyses of purified GPL-S8. The results showed that GPL-S8 contained a 4,6-*O*-(1-carboxyethylidene)-3-*O*-methyl-Glc residue and two main pseudomolecular ions (*m/z* 1,565.9 and 1,579.8 $[M + Na]^+$) (data not shown). Consequently, as shown in Fig. 5, these results were consistent with the proposed structure for GPL-S8-1 and -2 containing 4,6-*O*-(1-carboxyethylidene)-3-*O*-methyl-Glc, with differences in pseudomolecular ions due to fatty acid methylation.

DISCUSSION

Structural diversity of the ssGPLs, notably in their sugar residues, defines 28 serovars of MAC. Although these ssGPLs are known to contribute to the virulence of MAC, the mechanisms of their biosynthetic regulation are largely unknown. In this study, we clarified the biosynthetic pathway for serovar 8-specific GPL, specifically the glycosylation step in which a Glc residue is transferred to the Rha residue of serovar 1-specific GPL.

To isolate the genomic region associated with the biosynthesis of serovar 8-specific GPL, we compared the GPL biosynthetic gene clusters in several MAC strains and found significant differences in the *gtfB-drrC* region. The segment flanking the 3′ end of the *gtfB-drrC* region includes several genes responsible for the serovar 1-specific GPL whose structure is found in all ssGPLs. On the other hand, it is experimentally

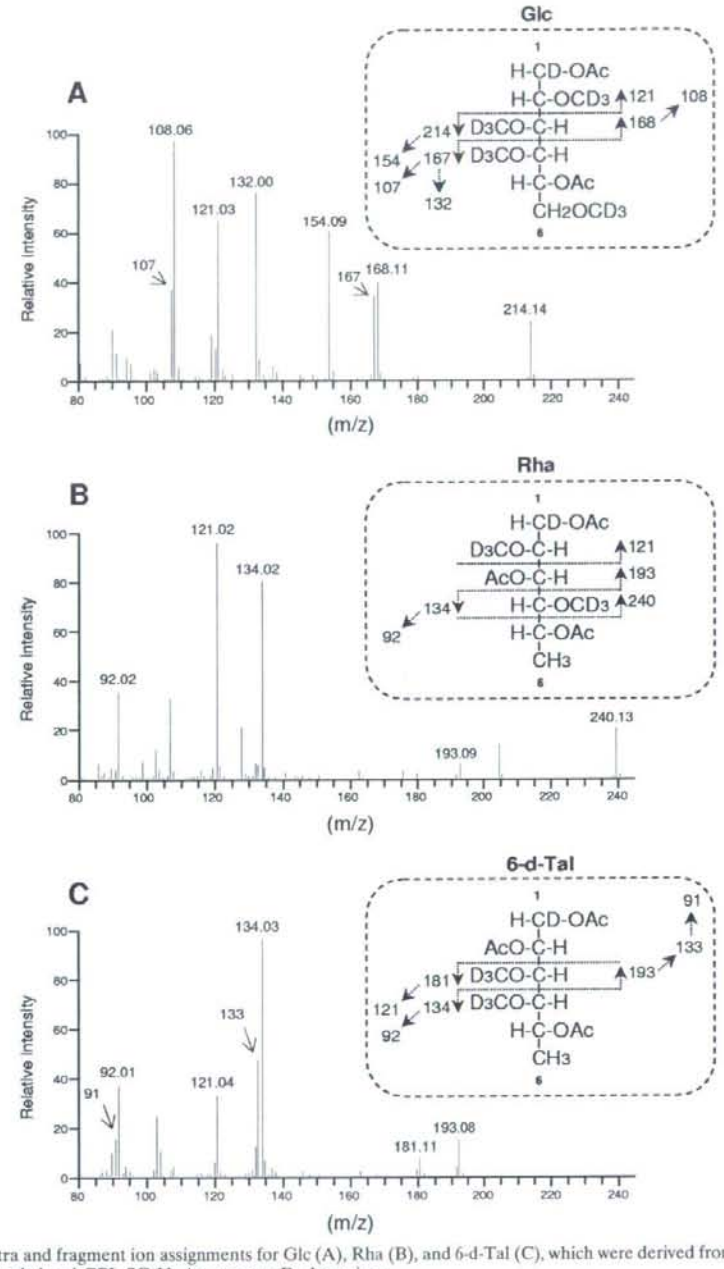

FIG. 4. GC-MS spectra and fragment ion assignments for Glc (A), Rha (B), and 6-d-Tal (C), which were derived from alditol acetates of sugars released from deuteriomethylated GPL-SG-U. Ac, acetate; D, deuterium.

clarified that the *gtfB-drrC* regions of serovar 2-, 7-, and 16-specific GPL-producing strains contain the genes involved in the formation of the specific sugar residues that are transferred to the Rha residue of serovar 1-specific GPL (18, 19, 30). Thus, this region could play an important role in generating the structural diversity of ssGPLs. As shown in this study, the specific functions for formation of sugar moieties of serovar 8-specific GPL were due to the genes present in the *gtfB-drrC*